Low Field Electron Transport In A GaAs/GaAlAs Superlattice

by
Imtiaz Dharssi

A thesis submitted for
the degree of Doctor of Philosopy.
Department of Physics,
University of Warwick.
October 1990

Contents

List of Figures

Acknowledgments

I wish to express my gratitude to the following people:

Professor P.N. Butcher for his excellent supervision;

My fellow PhD students, especially Dr M. J. Smith and Dr V. Karavolas for being such good friends;

and in particular to my parents, for their constant support and encouragement.

Declaration

Unless stated otherwise, the work in this thesis is the authors' own original research, performed in the Department of Physics at the University of Warwick between October 1987 and September 1990 under the supervision of Professor P.N. Butcher. Some of the work has been published previously:

1. 'The effect of phonon confinement on perpendicular electron transport in a *GaAs/GaAlAs* superlattice', Dharssi I. and Butcher P.N. (1990) *J. Phys. Condens. Matter* **2** 119,

2. 'Interface roughness scattering in a superlattice', Dharssi I. and Butcher P.N. (1990) *J. Phys. Condens. Matter* **2** 4629,

3. 'Mobility and Hall factor calculations for a superlattice', Dharssi I., Butcher P.N. and Warren G. (to be published) *Superlatt. Microstruct.*,

and presented as posters at conferences

1. 'Interface roughness scattering in a superlattice', Dharssi I. and Butcher P.N., *I.O.P. Solid State Physics Conference* 1989 (Warwick).

2. 'Interface roughness scattering in a superlattice', Dharssi. and Butcher P.N., *Conference of the Condensed Matter Division of the E.P.S.* 1990 (Lisbon).

3. 'Mobility and Hall factor calculations for a superlattice', Dharssi I., Butcher P.N. and Warren G., *International conference on superlattices and microstructures* 1990 (East Berlin).

Summary

This thesis presents some results of low field mobility and Hall factor calculations in a $GaAs/Ga_{0.7}Al_{0.3}As$ superlattice. There is much experimental evidence that for a superlattice with a large enough miniband width, the electron transport proceeds by extended Bloch states and consequently the Boltzmann transport formalism is used. For these calculations polar optical phonon scattering and interface roughness scattering are considered.

Early calculations assumed the vibrational modes of a superlattice to be unperturbed by the superlattice structure. However the optical vibrational modes of a thin layer structure deviate strongly from those of the corresponding bulk materials. This effect is included in these calculations by using the dielectric continuum model and is found to increase the predicted mobility by up to a factor of two.

This predicted polar optical phonon limited mobility is however, much larger than the experimentally measured mobility. By including interface roughness scattering agreement with experiment is significantly improved. For a superlattice grown without growth interruptions at the interfaces the interface roughness scattering dominates electron transport in the growth direction and is of similar importance to polar optical phonon scattering for transport parallel to the layers. The effect of growth interruptions is investigated and is found to reduce interface roughness scattering.

Finally the Hall factors are calculated, the superlattice has two independent Hall factors both of which remain close to one.

Chapter 1

Introduction

1.1 Low Dimensional Structures

Advances in crystal growth techniques, in particular the development of molecular-beam epitaxy (MBE) and metal-organic chemical vapour deposition (MOCVD) techniques, have made possible the growth of semiconductors structures with controlled changes in the composition and doping on an atomic scale. This has lead to the realisation of a whole new class of materials.

It is possible to grow structures where the mobile charge carriers are constrained by potential barriers in one or more spatial dimensions. For example, if we consider an electron gas constrained in one spatial dimension in a potential well. When the well width becomes comparable to or less than the de Broglie wavelength of the electrons, the electrons have quantized energy levels in one spatial direction. The electron wave-vector in the direction of the confining potential is no longer a good quantum number. Thus the electrons move freely in two spatial dimensions but not in the third. It is also possible to grow structures where the electrons move

freely only in one or even zero spatial dimensions. These 'artificial' structures, commonly referred to as low-dimensional structures, show novel and interesting transport properties due to the reduced dimensionality of the carriers.

Transport properties radically different from those observed in bulk materials are also obtained when the feature size of the sample becomes small compared to some characteristic length scale of the system being considered (e.g. mean free path, inelastic scattering length, cyclotron radius of electrons in a high magnetic field etc). These systems have also come to be known as low-dimensional structures.

Much of the early work on low dimensional systems concerned the study of a two dimensional electron gas formed at the silicon-silicon dioxide interface in an n-channel MOSFET. Interesting effects such as as the Quantum Hall effect (von Klitzing et al, 1980) and weak localization (Bishop et al, 1985) have been observed in such systems. A comprehensive review of the work done in this system is given by Ando Fowler and Stern (1982). A 2-dimensional electron gas may also be formed in a heterojunction such as a GaAs/AlGaAs heterojunction. Grown using MBE or MOCVD growth techniques, a single interface exists between the GaAs and the AlGaAs and the electrons become confined in an inversion layer at the interface. Extremely high electron mobilities, typically $10^6 cm^2 V^{-1} s^{-1}$, have been measured at liquid helium temperatures in GaAs/AlGaAs heterojunctions. This is because of the dramatic reduction of electron scattering by the ionised donor atoms, due to a technique known as modulation doping, compared to that in bulk GaAs. Thus, due to the generally higher quality samples obtained with GaAs/AlGaAs heterojunctions, further new effects have been observed such as the fractional quantum Hall effect and ballistic motion. A 2-dimensional electron gas is also formed in a

single quantum well such as an AlGaAs/GaAs/AlGaAs system where a thin layer of GaAs is sandwiched between two thick layers of AlGaAs. The conduction band edge in GaAs lies at a lower energy than the conduction band edge of AlGaAs, thus the GaAs acts as a quantum well and the AlGaAs a potential barrier for the electrons. The electrons are thus confined in the GaAs well. Mobilities in a single quantum well are not as high as those found for a single heterojunction. This may be because of the poor quality of the interface formed by growing GaAs on AlGaAs and the subsequent scattering of the electrons by the interface roughness. A review of Electron transport in low-dimensional structures is given by Harris et al (1989).

The next class of material is the multiple quantum wells system. Here the well widths and barrier widths can be varied throughout the system. The wells are essentially independent of one another, each well contributing independently to the transport parallel to the interfaces. Electron transport perpendicular to the interfaces (Vertical Transport) is via hopping or resonant tunneling. A discussion of vertical transport and possible device applications is given by Capasso et al (1986).

1.2 Superlattices

The idea of the semiconductor superlattice was first proposed by Esaki and Tsu (1970). The superlattice structure consists of a periodic sequence of ultra-thin layers of alternating composition (e.g. GaAs/GaAlAs), of alternating doping (e.g. n-GaAs/ p-GaAs) or of alternating composition and doping. The first successful growth of a superlattice was reported by Chang et al (1973). Due to the very small lattice -constant mismatch between GaAs and GaAlAs the first superlattices were

based on these materials. Improvements in epitaxial growth techniques have made possible the study of new material systems exhibiting qualitatively new physical effects.

Superlattice structures, such as the GaAs/GaAlAs system, where one material acts as a quantum well for both electrons and holes are known as type I compositional superlattices. For the type II compositional superlattice one material acts as the quantum well for the electrons and the other material acts as the quantum well for the holes, thus there is a spatial separation between the electrons and holes. An example of a type II compositional superlattice is the $Ga_xIn_{1-x}As/GaAs_ySb_{1-y}$ system, the alloy composition x and y can be chosen so that the two materials are lattice-matched. Adjusting x and y the conduction band edge of $Ga_xIn_{1-x}As$ can be made higher or lower than the valence band edge of $GaAs_ySb_{1-y}$ resulting in a semiconductor-semimetal transition if the layers are sufficiently thin (Sai-Halasz, 1978). Doping superlattices also exhibit a spatial separation between the electrons and the holes. Recently there has been much interest in lattice-mismatched superlattices (e.g. Si/SiGe). The lattice-constant mismatch is accommodated by strain in the layers with few misfit defects generated if the layers are sufficiently thin. Reviews of various properties of superlattices are given by Ploog and Dohler (1983), Esaki(1985) and Osbourn et al (1987).

1.3 Superlattice Electronic Structure

The electronic structure of a superlattice as well as depending on the constituent materials is strongly dependent on the layer thickness and doping profile. Since

these can be precisely controlled it is possible to design the electronic band structure and this has lead to the idea of band gap engineering (Capasso, 1987). Thus the transport and optical properties can be tailored for a specific device application, or to exhibit new physical phenomena.

Many of the interesting properties of the superlattice arise from the splitting of the original bulk conduction and valence bands into narrow mini-bands. This splitting is due to the new increased periodic length of the superlattice and the subsequently narrow Brillouin zone in the growth direction. Calculation of this mini-band structure has raised interesting problems in basic physics such as band-gap alignment and matching of envelope functions at interfaces. There are many methods for the calculation of mini-band structures such as first principle calculations, the empirical psuedopotential method or the tight-binding model. A review of these methods is given by Smith and Mailhiot (1990). However the most widely used model is the effective -mass approximation. This, because of its simplicity, is the method used here to calculate the mini-band structure of a GaAs/AlGaAs superlattice.

A good description of the effective mass theorem applied to a superlattice is given by Vigneron (1988) and the main results are quoted here. The effective mass Hamiltonian for the superlattice electrons is given as

$$-\frac{\hbar^2}{2}\nabla\left(\frac{1}{m^*(z)}\nabla\right)F(\mathbf{r})+V_{SL}(z)F(\mathbf{r})=\epsilon_k F(\mathbf{r}) \qquad (1.1)$$

where $F(\mathbf{r})$ is the envelope wavefunction. The unusual form of the kinetic energy term in (1.1) is necessary to make the Hamiltonian hermitian and obtain continuous current density at an interface now that the effective mass is a function of position.

The boundary conditions are also modified, so we have the conditions that

$$F(\mathbf{r}) \quad and \quad \frac{1}{m^*(z)}\frac{\partial F}{\partial z} \tag{1.2}$$

are continuous at an interface. The superlattice potential $V_{SL}(z)$ is given by (1.3).

$$V_{SL}(z) = \begin{cases} 0 & in\ a\ GaAs\ layer \\ V_0 & in\ an\ AlGaAs\ layer \end{cases} \tag{1.3}$$

The origins of this periodic potential are easy to understand. The conduction band electrons in GaAs (AlGaAs) behave as though they move in a constant potential $\epsilon_c^{GaAs}(\epsilon_c^{AlGaAs})$ which is the energy of the Γ conduction band edge in GaAs(AlGaAs) and so $V_0 = \epsilon_c^{AlGaAs} - \epsilon_c^{GaAs}$. Thus in a superlattice we obtain a Kronig-Penney potential with the same periodicity as the superlattice. The above treatment is restricted to the case when the superlattice electron wavefunction is made up of bulk states from one conduction band. A more general treatment when band mixing becomes important is given by Bastard (1982,1983).

We can solve the Kronig-Penney model exactly, but to obtain analytical results we use the tight-binding theory. In the nearest neighbor approximation the envelope wavefunction is written

$$F(\mathbf{r}) = \left(\frac{l}{V}\right)^{1/2} \exp(i\mathbf{k}_\parallel.\mathbf{x}_\parallel) \sum_n \phi(z - nl) \exp(ik_z nl) \tag{1.4}$$

where $\mathbf{k}_\parallel = k_x\hat{i} + k_y j$ and $\mathbf{x}_\parallel = x\hat{i} + yj$. $\phi(z)$ is the normalised eigenfunction of the Hamiltonian for a single potential well of width 2a and barrier height V_0 centered at z=0 (Appendix 1). The normalization constant in (1.4) is derived for the case when the overlap from adjacent wells is ignored i.e.

$$\phi(z - nl)\phi(z - ml) = \delta_{n,m}\phi^2(z - nl). \tag{1.5}$$

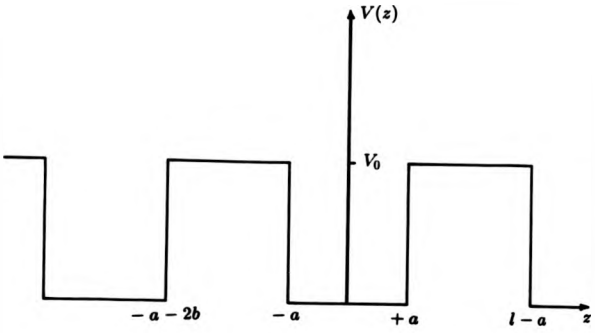

Figure 1.1: Kronig-Penney potential.

The mini-band structure in the nearest neighbor approximation can be written as

$$\epsilon_k = \frac{\hbar^2 k_\parallel^2}{2m_\parallel^*} + \Delta(1 - \cos k_z l) \tag{1.6}$$

where 2Δ is the miniband width, Using the same method as Palmier and Chomette (1982) and Warren and Butcher (1986) the mini-band width is calculated from the superlattice dispersion relation, when $\mathbf{k}_\parallel = 0$:

$$\cos k_z l = \cos(2k_a a)\cos(2k_b b) - \frac{1}{2}\left(\alpha + \alpha^{-1}\right)\sin(2k_a a)\sin(2k_b b), \tag{1.7}$$

where

$$\alpha = \frac{m^*_{GaAs} k_a}{m^*_{AlGaAs} k_b} \tag{1.8}$$

$$k_a^2 = \frac{2m^*_{GaAs}\epsilon_k}{\hbar^2} \tag{1.9}$$

$$k_b^2 = \frac{2m^*_{AlGaAs}}{\hbar^2}(\epsilon_k - V_0). \tag{1.10}$$

Before any calculations of the miniband width can be made the conduction band offset V_0 must be known. While the difference in the band gap of the two materials ΔE_g is well known, there has been controversy as to what fraction of this difference (ΔE_g) appears in V_0. Fractions ranging from 50 % to 80 % have been quoted. More recently experimentally determined values in the range 60% to 70% have become widely accepted, Ab initio calculations are also in agreement with these figures (Bylander and Kleinman, 1987). We use the experimental results of Okumara et al (1985) that $V_0 = 0.67\Delta E_g = 831 x meV$. All the results in this thesis are given for a $GaAs/Ga_{0.7}Al_{0.3}As$ superlattice and we put $V_0 = 250meV$. To simplify the calculation the small difference in effective mass between the GaAs and GaAlAs layers is ignored and we put $m_\parallel^* = m^*_{GaAs}$.

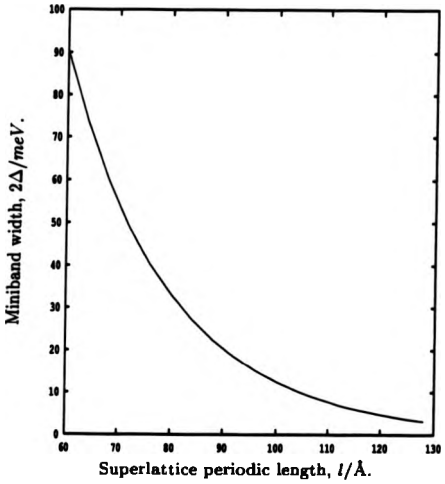

Figure 1.2: The superlattice miniband width.

The miniband width 2Δ is plotted as a function of the superlattice periodic length l for a conduction band offset of $V_0 = 250meV$.

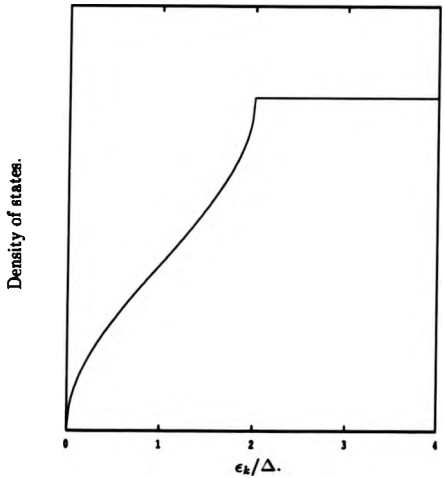

Figure 1.3: Density of states.

The density of states for the lowest electron miniband of the superlattice is shown. Note the critical point in the density of states at $\epsilon_k = 2\Delta$.

Before proceeding further it is worthwhile examining the validity of the simple effective mass model used here. This was first tested by optical absorption measurements in GaAs/GaAlAs multiple quantum wells (MQW), Dingle et al(1974,1975). Their results were in good agreement with those predicted by the effective mass theorem. Another study probed the electron probability density in a GaAs/GaAlAs quantum well. One plane of cations were substituted with either Indium or Aluminum. Optical determination of the energy levels as function of the position of this highly localized perturbation were used to determine the electron probability density, and the results also confirm the validity of the effective mass theorem (Marsin and Gerard 1989). The mini-band structure has been calculated using more sophisticated microscopic models (see Smith and Mailhiot 1990 and references therein). These show that while the effective mass model does not reproduce all the interesting electronic properties of a superlattice it is in most cases adequate for transport calculations.

We use the results of Munoz et al (1989) to illustrate when the effective mass theorem is applicable. The electronic structure was calculated for a GaAs/AlAs superlattice and the results should be qualitatively similar for a GaAs/GaAlAs superlattice. When considering the lowest lying electron mini-band four separate regions exhibiting different behavior were identified(fig 1.4). When both the GaAs and AlAs layers are very narrow the effective mass theorem completely breaks down (region IV). This is because our assumption that the envelope wavefunction is slowly varying over unit cells of GaAs and AlAs is no longer correct. In region II the electrons in the lowest lying mini-band are confined to the AlAs layers. These electrons are associated with bulk X states and the X conduction band edge is lower in AlAs than

in GaAs. In region III there is strong mixing between bulk Γ and X states. The electron envelope wavefunction is significant is both the GaAs and AlAs layers. The effective mass model used here is applicable in region I. The electrons are associated with bulk Γ states and are confined in the GaAs layers.

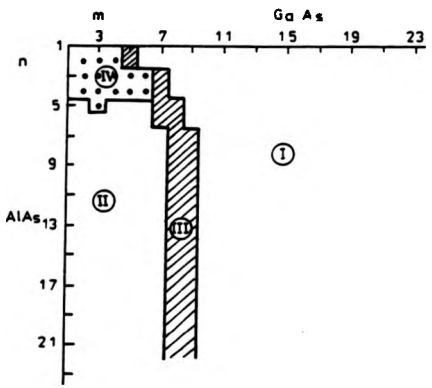

Figure 1.4: Four distinct regions of the superlattice miniband structure. Munos et al (1989) identify four separate regions for *GaAs/AlAs* superlattices which show qualitatively different behavior when considering the lowest lying electron miniband. The label $m(n)$ denotes the number of monolayers in a *GaAs(AlAs)* slab of the superlattice. The labels I...IV are explained in the text. Figure reproduced from Munos et al (1990).

Chapter 2

Transport Theory

2.1 Introduction

When an electric field or thermal gradient is applied to a solid state system there will be a net flow of charge, mass or energy. Here we introduce the ideas and methods for examining the transport properties of a crystalline material. The requirement is for an approach that gives an insight into the physical processes involved in the transport of charge or heat which is simpler then a full quantum mechanical treatment but is also reasonably accurate. The formulations most generally used are essentially classical in nature in that they treat the carriers as having a well defined positions and momenta. The simplest of these formulations is the kinetic method where the motion of an average carrier is followed with a simple treatment of scattering. A more accurate treatment is given by the Boltzmann transport equation and this is the method described in this chapter.

Before considering the transport theory in a superlattice, it is worthwhile discussing electron transport in bulk semiconductor crystals. Many aspects of this are

well understood and a good description is given by Smith et al (1967), Butcher(1973). For calculations of the transport properties it is a practical necessity to make use of the one-electron approximation in which the effective one-electron Hamiltonian is obtained by treating the electron-electron interaction only in an approximate manner. It is then possible to consider the motion of an electron in the combined crystalline and external fields. This is done within the framework of the effective mass theorem. The theorem shows that for many situations of interest in transport theory 'the effect of the external fields on a solid can be discussed in terms of the motion of classical particles in these fields'(Smith 1967). However the mass of one such particle will be different from the free electron mass and will in general depend on its momentum. To formulate the equations of motion for the particle a wavepacket is considered and the equations which govern the time development of the average dynamical variables associated with the wavepacket are determined. The wavepacket is constructed from the one-electron Bloch states (centered around $\mathbf{k} = \mathbf{k_0}$) in a single band which is assumed to be non-degenerate.

$$\Psi = \sum_{\mathbf{k}} a(\mathbf{k}, t)\Psi_{n,\mathbf{k}}(\mathbf{r}). \tag{2.1}$$

The classical equations of motion of the wavepacket are then given by

$$\begin{aligned} \dot{\mathbf{r}} &= \mathbf{v}_{\mathbf{g}} = \hbar^{-1}\nabla_{\mathbf{k}}\epsilon_n(\mathbf{k}) \\ \hbar\dot{\mathbf{k}}_0 &= -e(\mathbf{E} + \mathbf{v} \times \mathbf{B}). \end{aligned} \tag{2.2}$$

These equations are valid provided inter-band scattering is negligible and the dimensions of the wavepacket are small enough such that the applied fields hardly vary over the breadth of the wavepacket and yet the wavepacket is also highly localised in reciprocal space.

Using the above results it is now possible to determine the macroscopic currents generated in the presence of external fields. Since we are interested in average effects it would be pointless to consider the detailed motion of each particle in the system. Rather a statistical procedure is called for and a distribution function $f(\mathbf{k},\mathbf{r},t)$ is introduced. Here $f(\mathbf{k},\mathbf{r},t)$ gives the probability that a particle occupies a state k in the neighborhood of r at time t. As we are dealing with weakly interacting particles which obey the Pauli exclusion principle $f(\mathbf{k},\mathbf{r},t)$ is given by the Fermi-Dirac distribution function when the system is in equilibrium , ie when no external fields are applied. The effect of an applied field is to accelerate the particles and to drive the distribution function away from its equilibrium value. So far we have considered only a perfect crystal, however any real crystal contains disorder (eg lattice vibrations, impurities) which destroys the perfect periodicity of the crystal. The effect of this is to scatter the electrons from one state to another. The role of this scattering is to oppose the the response of the system to the applied fields and to attempt to return the system to equilibrium. The calculation of the new distribution function, taking into account the effect of the external fields and the scattering, can then be performed using the Boltzmann transport equation. Once the distribution function is known it is a simple matter to calculate the transport coefficients of the system. The electron density n and the electric current density J are given by

$$n = \frac{1}{4\pi^3}\int f(\mathbf{k},\mathbf{r},t)\,d\mathbf{k}$$

$$\mathbf{J} = \frac{-e}{4\pi^3}\int f(\mathbf{k},\mathbf{r},t)\mathbf{v}(\mathbf{k})\,d\mathbf{k} \qquad (2.3)$$

Many calculations have been performed for transport in bulk crystalline materials

with results in good agreement with experiment, (e.g. fig. 2.1).

2.2 Transport in a Superlattice

Semiconductor superlattices are ideal structures in which to study transport properties. By adjusting the composition and the well and barrier thickness it is possible to explore a range of transport processes from Bloch transport to hopping or resonant tunneling. Many of the interesting transport properties occur when the field is applied in the growth direction (vertical transport) and attention is focussed on this case.

The first study of electron transport in a superlattice was performed by Esaki and Tsu (1970). They assumed that the electron transport proceeds by extended Bloch states and used a kinetic model. Following their approach and using the classical equations of motion (2.2), we find that

$$\begin{aligned} v_z &= \hbar^{-1}\Delta l \sin(k_z l) \\ k_z(t) &= k_z(0) - eE_z t/\hbar \end{aligned} \tag{2.4}$$

when a steady electric field E_z is applied in the direction perpendicular to the layers (z direction). Thus the velocity increment in a time interval dt is given by

$$dv_z = \frac{eE_z}{\hbar^2}\Delta l^2 \cos(k_z l)\, dt. \tag{2.5}$$

Taking into account any electron scattering in a simple manner, the average drift velocity when collisions occur with a frequency τ^{-1} is given by

$$v_d = \int_{t=0}^{t=\infty} \exp(-t/\tau)\, dv_z. \tag{2.6}$$

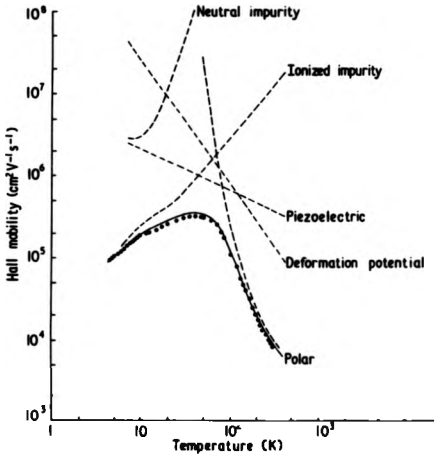

Figure 2.1: The Hall mobility of n-GaAs.

The broken curves give the mobilities calculated for the scattering process indicated acting in isolation. The full curve is the overall Hall mobility taking all scattering processes into account and is in good agreement with the experimental points. Note that above 100 K the electron scattering is dominated by polar optical phonons. Figure reproduced from Fletcher and Butcher (1972).

Remembering that k_z is a function of time, it is found that

$$v_d = \frac{\pi \Delta l}{\hbar} \frac{\zeta}{1 + \pi^2 \zeta^2} \tag{2.7}$$

where $\zeta = eE_z \tau l / \pi \hbar$. Thus the drift velocity versus field in the growth direction has a maximum at $\pi\zeta = 1$ and a negative differential velocity (NDV) is predicted when the scattering time or the electric field E_z is large enough. If the scattering time is sufficiently long the electrons may be expected to exhibit Bloch oscillations. Thus if an electron can traverse the reduced Brillouin zone without being scattered it's velocity will be an oscillatory function of time and the electron will perform oscillations in real space. Since a superlattice has a much narrower Brillouin zone than a bulk crystal in the growth direction it should be easier to observe Bloch oscillations in a superlattice. The condition for observing Bloch oscillations is that $\zeta > 2$, this is approximately six times more difficult to achieve than negative differential velocity. Bloch oscillations have, as yet, not been observed. It may be that the large fields required allow interband transitions at the Brillouin zone edge rather than causing Bragg reflections. Also the unavoidable interface roughness will cause electron scattering to increase. A fuller discussion of the validity and conditions of observation of Bloch oscillations is given by Grondin at al (1985).

Other mechanisms for negative differential conductivity have been proposed. Tsu and Dohler (1975), suggested that if a large electric field is applied along the superlattice axis (z direction) it can induce localization of the electron states in the growth direction. This occurs when $elE_z \cong \Delta$. When the electron have extended states transport is by Bloch conduction, however if the electron states are localized transport is by longitudinal optical phonon assisted hopping. The transition from Bloch

to hopping transport resulting in a reduction of the electron mobility. However the first experimental observation of negative differential conductivity in a superlattice was explained by yet another mechanism: Esaki and Chang (1974). The electric field is again applied in the growth direction. For low fields, transport is assumed to be by Bloch conduction however at larger fields the unavoidable non-uniformity in the superlattice structure is assumed to lead to the formation of a microscopic high field domain. The negative differential conductivity is then a result of resonant tunneling through this high field domain.

Calecki et al (1984) have questioned the assumption that, at least for low fields, electron transport in the growth direction occurs by extended Bloch states. If the disorder in a superlattice is sufficiently large then the electron states will be localized. The criteria for the amount of disorder required to cause localization in the growth direction is given approximately by

$$\hbar/\tau > \Delta \qquad (2.8)$$

i.e localization occurs when the collision broadening is greater than the mini-band width. When the electrons states are localised, transport is by longitudinal optical phonon assisted hopping. Calecki et al (1984) calculate the electron mobility in the growth direction for the hopping case and find their predicted results in good agreement with experimental values. While the mobility calculated assuming Bloch transport and using the Boltzmann transport equation (Palmier and Chomette, 1982) are two orders of magnitude larger than the hopping mobility.

However, in the last few years, many convincing demonstrations of Bloch transport in a superlattice have been given using techniques as diverse as cyclotron reso-

nance (Duffield et al 1986), optical time of flight (Deveaud et al 1988), hot electron spectroscopy (England et al 1989) and mobility measurements (Sibille et al 1987). A transition from Bloch to hopping transport in a superlattice has also been observed. The Bloch conductivity is inversely proportional to the scattering rate and considering electron-longitudinal optical phonon scattering, the Bloch mobility decreases with increasing temperature. On the other hand, the hopping mobility is proportional to the electron - longitudinal optical phonon scattering rate and thus increases with temperature. Sibille et al (1987) identified the Bloch to hopping transition from a minimum in the mobility vs temperature curve. It has also become possible to obtain negative differential velocity in a superlattice at room temperature (Sibille et al 1989a, 1989b). The peak velocity and critical field for this negative differential velocity have been measured as a function of mini-band width (Sibille et al 1990). From these results, for superlattices with mini-band widths greater than $50meV$ the negative differential velocity was interpreted as due to the mechanism originally proposed by Esaki and Tsu (1970) while for narrow minibands the results indicate electric field induced localisation as the mechanism.

2.3 Boltzmann Transport Equation

Since transport in a superlattice can proceed by extended Bloch states it is appropriate to use the Boltzmann transport equation to calculate transport coefficients for this system. The Boltzmann transport equation is derived using the classical equations of motion (2.2) and assuming conservation of electrons. The resulting equation is then used to obtain the distribution function $f(\mathbf{k}, \mathbf{r}, t)$ which has been

discussed previously. The full derivation of the Boltzmann transport equation is given by Butcher(1973), and the equation is simply quoted here

$$\frac{\partial f}{\partial t} + \mathbf{v}.\nabla f + \hbar^{-1}\mathbf{F}'.\nabla_{\mathbf{k}} f = \left(\frac{\partial f}{\partial t}\right)_{COLL} \tag{2.9}$$

where $\mathbf{F}' = -e[\mathbf{E} + \mathbf{v} \times \mathbf{B}] - \nabla\epsilon(\mathbf{k})$. The above equation includes the diffusion of electrons in real space and the drift of electrons in velocity space due to the applied fields. The term on the right hand side is necessary to include the interaction of an electron with any disorder in the system, phonons, charged impurities etc. . It is supposed that the effect of these interactions is to induce transitions between the electron states and thus we write

$$\left(\frac{\partial f}{\partial t}\right)_{COLL} = \int \{P(\mathbf{k}', \mathbf{k}) f(\mathbf{k}')[1 - f(\mathbf{k})] - P(\mathbf{k}, \mathbf{k}') f(\mathbf{k})[1 - f(\mathbf{k}')]\}\, d\mathbf{k}' \tag{2.10}$$

where $8\pi^3 V^{-1} P(\mathbf{k}, \mathbf{k}')$ is the scattering rate from a full state $\mathbf{k}$ to an empty state $\mathbf{k}'$. We are interested in the case when the applied electric field is small and no magnetic field present. Hence we write the distribution function as

$$f(\mathbf{k}) = f_0(\mathbf{k}) + g(\mathbf{k}) \tag{2.11}$$

where $g(\mathbf{k})$ is a small perturbation to the equilibrium Fermi-Dirac distribution function $f_o(\mathbf{k})$. Substituting (2.11) into the Boltzmann transport equation and ignoring second and higher order terms in $g(\mathbf{k})$ the linearized Boltzmann transport equation is obtained:

$$-\frac{e}{\hbar}\mathbf{E}.\nabla_{\mathbf{k}} f_0 = \left(\frac{\partial g}{\partial t}\right)_{COLL}. \tag{2.12}$$

2.3.1 Relaxation Time Approximation

The simplest method to solve the Boltzmann transport equation is to use the relaxation time approximation which assumes

$$\left(\frac{\partial g}{\partial t}\right)_{COLL} = -\frac{g(\mathbf{k})}{\tau_r}. \tag{2.13}$$

Where $\tau_r(\mathbf{k})$ is the relaxation time. After some manipulation the form for the relaxation time is obtained (Butcher, 1973)

$$\tau_r^{-1} = \int \frac{1-f_0'}{1-f_0} P(\mathbf{k},\mathbf{k}') \left[1 - \frac{\tau_r' \mathbf{v}'.\mathbf{E}}{\tau_r \mathbf{v}.\mathbf{E}}\right] d\mathbf{k}', \tag{2.14}$$

where $f_0' = f_0(\mathbf{k}')$. Since τ_r occurs on both sides of (2.14), the relaxation time approximation is only useful when the term in square brackets reduces to a simple form. This occurs when the collisions are $\mathbf{k}$ randomizing ie $P(\mathbf{k},\mathbf{k}') = P(\mathbf{k},-\mathbf{k}')$. The only other case is when the scattering is elastic and the energy band is spherically symmetric. However the energy band in a superlattice is highly anisotropic and in general many scattering mechanisms are not $\mathbf{k}$ randomising thus a different method is needed.

2.3.2 The Iterative Method

When the relaxation time approximation does not lead to a solution for the perturbed distribution function an iterative technique may be used. This is based on an algorithm developed by Rode (1970). The linearised Boltzmann transport equation can be rearranged into the form

$$g(\mathbf{k}) = \frac{\int \{g'[(1-f_0')P(\mathbf{k}',\mathbf{k}) + f_0 P(\mathbf{k},\mathbf{k}')]\}\, d\mathbf{k}' + e\hbar^{-1}\mathbf{E}.\nabla_k f_0}{\int \{f_0' P(\mathbf{k}',\mathbf{k}) + (1-f_0')P(\mathbf{k},\mathbf{k}')\}\, d\mathbf{k}'} \tag{2.15}$$

where $g' = g(\mathbf{k}')$. $g(\mathbf{k})$ is obtained from the above equation by guessing an initial form for $g(\mathbf{k})$ and iterating until convergence is obtained. If the initial choice is $g(\mathbf{k}) = 0$ then the first iteration gives

$$g_1(\mathbf{k}) = e\hbar^{-1}\tau(\mathbf{k})\mathbf{E}.\nabla_k f_0 \tag{2.16}$$

where $\tau(\mathbf{k})$ is the lifetime of an electron state $\mathbf{k}$ which is given by

$$\tau^{-1}(\mathbf{k}) = \int P(\mathbf{k}', \mathbf{k})\, d\mathbf{k}'. \tag{2.17}$$

Thus the first iteration would give the same answer as assuming that the relaxation time is equal to the lifetime of the electron state, ie $\tau_r(\mathbf{k}) = \tau(\mathbf{k})$. The main point is that in (2.17) the 'scattering in' terms have been neglected (i.e. the electron scattering back into the volume element $d\mathbf{k}$). When the 'scattering in ' terms are included this can lead to a significant increase in the predicted mobilities. Thus the assumption that the relaxation time is the same as the electron lifetime can lead to errors of up to an order of magnitude.

Chapter 3

Electron Scattering

3.1 Introduction

We have discussed in the previous chapter a method of calculation of classical transport effects. The motion of an electron in a perfect crystal is unhampered and for electrons in a perfect crystal with a parabolic energy band the application of an external electric field would uniformly accelerate the electrons causing a linear increase of the electron drift velocity in time. However, in any real crystal the drift velocity of the electron gas always remains at a finite value which, for sufficiently small applied fields, is proportional to the strength of the applied field. This finite value of the electron drift velocity is due to electron interactions with imperfection in the crystalline material. These interactions are assumed to be weak so that they can be treated as a perturbation and that the effect of the interactions is to induce transitions between the one electron Bloch states. Thus, these interactions are usually referred to as scattering or collision processes. For the calculation of transport properties an understanding of these scattering processes is therefore essential.

Imperfections in a crystal are produced in many ways. One form of deviation from a perfectly periodic structure is that produced by a random array of static defects such as dislocation, neutral impurities or charged impurities. Often impurities have to be introduced deliberately to dope the semiconductor crystal. Of these scattering mechanisms charge impurity scattering is usually the most important. In this case the presence of the charged impurity causes a perturbation in the electrostatic potential which scatters the electrons. However charged impurity scattering ceases to be important for high energy electrons and for this process the relaxation time in bulk materials $\tau_e \propto \epsilon^{3/2}$. Physically this behavior arises because the higher the electron velocity the smaller the angle through which the electron is scattered. Thus charged impurity scattering is only important at low temperatures. In mixed semiconductors such as *GaAlAs* an additional scattering mechanism is alloy scattering. We have used the virtual crystal approximation for the *GaAlAs* layers of a superlattice to calculate the miniband structure. However in *GaAlAs* the *Ga* and *Al* atoms are randomly distributed over the cation sites. Consequently the electrons will experience fluctuations of the local potential and this will lead to scattering of the electrons. For a *GaAs/GaAlAs* superlattice, since the electron envelope function is mostly confined within the *GaAs* layers, this scattering mechanism is not expected to be important.

Another interaction of interest is that due to lattice vibrations. In calculating the energy band structure of a crystal it is assumed that the atoms in the crystal are frozen in their equilibrium position. However at any finite temperature the atoms will vibrate about their equilibrium positions and thus the crystal potential will vary with time and scatter the electrons. If the atoms make small oscillations

about their equilibrium positions we can use the harmonic approximation and the potential energy term in the Hamiltonian for the atomic motion will be a quadratic. By introducing new coordinates it is possible to decompose the coupled lattices vibrations into a system of independent harmonic oscillators (Maradudin et al 1971, Bruesch 1982). These new coordinates are known as normal coordinates. With each normal coordinate is associated an independent harmonic oscillator which describes a particular mode of vibration of the crystal with a single frequency and wavevector. The vibrational modes are called normal modes and there are as many normal modes as there are degrees of freedom in the crystal.

The interaction of the electrons with the lattice vibrations is usually dealt with by adopting a quantum mechanical picture. Once the normal modes are obtained quantization of the lattice vibrations is simple and results in the energy and crystal momentum of each normal mode becoming quantized. Considering a single normal mode, its energy and crystal momentum are given by

$$\begin{aligned} \epsilon &= \hbar\omega(n + \tfrac{1}{2}) \\ \mathbf{p} &= \hbar\mathbf{q}(n + \tfrac{1}{2}), \end{aligned} \tag{3.1}$$

where n is a non-negative integer quantum number. The classical picture of the lattice vibrations is simply that as n is increased the energy and amplitude of the vibrations is increased. However since the energy and momentum can only change by multiples of a fixed amount, a different interpretation can be given (Inkson 1984). Ignoring the zero-point energy and momentum we can consider an oscillator at level n as being n oscillators at level 1. Changing the system from level n to level m would correspond to adding $m-n$ oscillators at level 1. Since the system can change only by adding or subtracting discrete packets of energy and momentum, the packets have a

particle like behavior. These particles are called phonons and have a definite energy and momentum associated with them. However phonons are not conserved, they may be created or destroyed and the number of phonons is given by the quantum number n. The equilibrium phonon population at a particular temperature is given by the Bose-Einstein formulae

$$n_q = [\exp(\hbar\omega_q/k_BT) - 1]^{-1}. \tag{3.2}$$

The phonons interact with the electrons as particles obeying the principle of conservation of energy and crystal momentum (to within a reciprocal lattice vector).

In a crystal structure such as *Si* or *GaAs* there are two atoms in each unit cell. Lattice vibrations in which the two atoms in each unit cell move in the same direction are known as acoustic modes. For acoustic modes, in the long wavelength limit (small q), the frequency of vibration is proportional to the phonon wavevector q and $\omega_q = v_s q$ where v_s is the speed of sound. In the simplest models there are three acoustic phonon modes, one corresponding to longitudinal vibrations and two modes corresponding to transverse vibrations. When the two atoms in the unit cell move in opposite directions we obtain optical phonon modes. In the long wavelength limit the displacement of the center of mass of a unit cell vanishes, the frequency of vibration is almost independent of the phonon wavevector and is non-zero. Again there are three optical modes, one longitudinal and two transverse. We can also distinguish between homopolar materials such as Si in which the two atoms in the unit cell are identical and heteropolar materials such as *GaAs* where the atoms in the unit cell are different and are partially ionized. Consequently, for a material such as *GaAs* it is also necessary to include the Coulomb forces between the ions in

the theory of the lattice vibrations.

In discussing electron-phonon scattering it is usual to use the continuum approximation which allows the introduction of macroscopic quantities such as strain, polarization and macroscopic electric field. The continuum approximation is adequate since it is the long-wavelength phonons which dominate the electron scattering. The electron-phonon interaction is divided up in accordance with the type of lattice vibrations with which the electrons interact and the nature of the perturbing potential associated with the lattice vibrations. The lattice vibrations change the spacing between the atoms in the crystal. The potential produced by this deformation of the crystal is called the deformation potential and is taken to be proportional to the strain produced by the vibrations. In crystals such as *GaAs* which lack inversion symmetry and where the atoms are partially ionised, a piezoelectric effect is exhibited. The strain due to the acoustic lattice vibrations generates an electric field and the scalar potential associated with the electric field scatters the electrons. The other important electron-phonon interaction is due to the longitudinal optical phonons. These modes, in heteropolar materials, also produce an electric field. Electron scattering by longitudinal optical phonons will be discussed in more detail in the following sections. A comprehensive discussion of electron scattering is given by Nag (1980).

3.2 Longitudinal Optical Phonon Scattering in Bulk GaAs

Longitudinal Optical (LO) phonons are the dominant electron scattering mechanism in bulk *GaAs* at room temperature, they may therefore be expected to be an important scattering mechanism in *GaAs/GaAlAs* superlattices. We begin with a discussion of LO phonon scattering in bulk *GaAs* as a prelude to LO phonon scattering in a superlattice. The quantity of interest for LO vibrations is the relative displacement

$$\mathbf{W} = \mathbf{u}_+ - \mathbf{u}_- \tag{3.3}$$

where $\mathbf{u}_+$ and $\mathbf{u}_-$ are the displacement of the positive and negatively charged ions, respectively. In quantized form the relative displacement is given by (Butcher 1986)

$$\mathbf{W}_{LO}(\mathbf{r}) = \sum_{\mathbf{q}} \left[\frac{\hbar}{2V\rho_r\omega_{LO}}\right]^{1/2} \frac{\mathbf{q}}{|\mathbf{q}|} \left[\exp(i\mathbf{q}.\mathbf{r})b_{\mathbf{q},LO} + \exp(-i\mathbf{q}.\mathbf{r})b^+_{\mathbf{q},LO}\right]. \tag{3.4}$$

$b_{\mathbf{q}}$ and $b^+_{\mathbf{q}}$ are the phonon annihilation and creation operators and correspond to the simple harmonic time dependent terms in the classical equation for the relative displacement. ρ_r is the reduced mass density, where the reduced mass of a unit cell is given by $M_r^{-1} = M_+^{-1} + M_-^{-1}$ and M_+, M_- denoting the mass of a positive and negative ion in the unit cell. As is usual for transport calculations we have ignored spatial dispersion of the LO modes, ie we have taken ω_{LO} to be independent of the phonon wavevector in (3.4).

To calculate the electron-LO phonon scattering rates it is necessary to calculate the electric fields associated with the LO modes. This is done using the Born and

Huang phenomenological equations (Born and Huang, 1962).

$$\begin{aligned} \rho_r \ddot{\mathbf{W}} &= -b_{11}\mathbf{W} - b_{12}\mathbf{E} \\ \mathbf{P} &= -b_{12}\mathbf{W} - b_{22}\mathbf{E}, \end{aligned} \tag{3.5}$$

where $\mathbf{E}$ and $\mathbf{P}$ are the macroscopic electric field and the polarisation, respectively. Maxwell's displacement vector is given by $\mathbf{D} = \epsilon_0\mathbf{E} + \mathbf{P} \equiv \epsilon_0\kappa(\omega)\mathbf{E}$. Rearranging (3.5) we can write

$$\mathbf{D} = \epsilon_0\mathbf{E} - \left[b_{22} - \frac{b_{12}^2}{\rho_r(\omega_{TO}^2 - \omega^2)}\right]\mathbf{E}. \tag{3.6}$$

Hence the dielectric constant $\kappa(\omega)$ can be written in the form

$$\kappa(\omega) = \kappa_\infty + \frac{\kappa_0 - \kappa_\infty}{1 - (\omega/\omega_{TO})^2} \tag{3.7}$$

where κ_0 is the static dielectric constant, and κ_∞ is the high frequency dielectric constant. We see from the above equation that $\kappa_\infty = 1 - b_{22}/\epsilon_0$, $\kappa_0 = \kappa_\infty + b_{12}^2/b_{11}\epsilon_0$ and $b_{11} = \rho_r\omega_{TO}^2$. κ_0, κ_∞ and ω_{TO} can all be determined from experimental data.

The frequency of the LO modes ω_{LO} can be derived from Maxwell's equations. In the absence of free charges and neglecting retardation

$$\nabla \times \mathbf{E} = 0\ ,\ \nabla.\mathbf{D} \equiv \kappa(\omega)\nabla.\mathbf{E} = 0. \tag{3.8}$$

These equations can only be satisfied if $\mathbf{E} = 0$ or $\nabla \times \mathbf{E} = 0$ and $\kappa(\omega) = 0$. The first case is associated with transverse optical (TO) modes which have no electric field associated with them. The second case gives us LO modes, and the frequency of the LO modes is given by $\kappa(\omega_{LO}) = 0$. From (3.7), this occurs when

$$\omega_{LO} = \omega_{TO}\left(\frac{\kappa_0}{\kappa_\infty}\right)^{1/2}. \tag{3.9}$$

Moreover from the Born and Huang equations (3.5) the relation between the relative

optical displacement and the electric field is given by

$$\mathbf{E}(\omega_q) = \mathbf{W}\rho_r^{1/2}\frac{\omega_q^2 - \omega_{TO}^2}{[\epsilon_0(\kappa_0 - \kappa_\infty)]^{1/2}\omega_{TO}} \tag{3.10}$$

and when $\omega_q = \omega_{LO}$,

$$\mathbf{E}_{\omega_{LO}} = \mathbf{W}\left(\frac{\rho_r}{\epsilon_0}\right)^{1/2}\left(\frac{1}{\kappa_\infty} - \frac{1}{\kappa_0}\right)^{1/2}\omega_{LO}. \tag{3.11}$$

The scalar potential associated with the electric field is given by

$$\mathbf{E} = -\nabla\nu \tag{3.12}$$

so that

$$\nu = \left(\frac{\hbar\omega_{LO}}{2V\epsilon_0}\right)^{1/2}\left(\frac{1}{\kappa_\infty} - \frac{1}{\kappa_0}\right)^{1/2}\sum_{\mathbf{q}} -\frac{1}{iq}[\exp(i\mathbf{q}.\mathbf{r})b_{\mathbf{q},LO} - \exp(-i\mathbf{q}.\mathbf{r})b_{\mathbf{q},LO}^+]. \tag{3.13}$$

The electron-LO phonon coupling term in the Hamiltonian is given by

$$H_{ep} = -e\nu \tag{3.14}$$

and the electron- phonon scattering rate is given by Fermi's golden rule

$$T(\mathbf{k}, n_{\mathbf{q}} \rightarrow \mathbf{k}', n_{\mathbf{q}}') = \frac{2\pi}{\hbar}\left|< \mathbf{k}', n_{\mathbf{q}}'|H_{ep}|\mathbf{k}, n_{\mathbf{q}} >\right|^2 \delta\{\epsilon_k' - \epsilon_k + (n_{\mathbf{q}}' - n_{\mathbf{q}})\hbar\omega_{\mathbf{q}}\}, \tag{3.15}$$

where $\mathbf{k}$ and $\mathbf{k}'$ are the initial and final electron states and $n_{\mathbf{q}}$ and $n_{\mathbf{q}}'$ are the initial and final phonon numbers. The annihilation and creation operators act on a phonon state $|n_{\mathbf{q}}>$ such that

$$\begin{aligned} b_{\mathbf{q}}|n_{\mathbf{q}}> &= n_{\mathbf{q}}^{1/2}|n_{\mathbf{q}} - 1> \\ b_{\mathbf{q}}^+|n_{\mathbf{q}}> &= (n_{\mathbf{q}} + 1)^{1/2}|n_{\mathbf{q}} + 1>. \end{aligned} \tag{3.16}$$

Thus, in the electron-LO phonon coupling term H_{ep}, the term containing the annihilation operator $b_{\mathbf{q},LO}$ corresponds to an electron absorbing a LO phonon, while

the term containing the creation operator $b^+_{q,LO}$ corresponds to an electron emitting a LO phonon. The scattering rate is only significant when the scattering process involves only a single phonon, ie $|n_q - n'_q| = 1$. Using the above results the scattering rate is determined to be

$$T(\mathbf{k} \rightarrow \mathbf{k}') = \frac{e^2 \pi \omega_{LO}}{V \epsilon_0} \left(\frac{1}{\kappa_\infty} - \frac{1}{\kappa_0}\right) \frac{1}{q^2} \{ n_q | < \mathbf{k}' | \exp(i\mathbf{q}.\mathbf{r}) | \mathbf{k} > |^2 \delta(\epsilon'_k - \epsilon_k - \hbar\omega_{LO}) + (n_q + 1) | < \mathbf{k}' | \exp(-i\mathbf{q}.\mathbf{r}) | \mathbf{k} > |^2 \delta(\epsilon'_k - \epsilon_k + \hbar\omega_{LO}) \} . \tag{3.17}$$

Since the electron envelope functions in bulk $GaAs$ are plane waves, the matrix elements have a simple form and we obtain conservation of crystal momentum

$$| < \mathbf{k}' | \exp(\pm i\mathbf{q}.\mathbf{r}) | \mathbf{k} > |^2 = \delta_{k-k', \pm q}. \tag{3.18}$$

Thus the final form of the electron-LO phonon scattering rate is given as

$$T(\mathbf{k} \rightarrow \mathbf{k}') = \frac{e^2 \pi \omega_{LO}}{V \epsilon_0} \left(\frac{1}{\kappa_\infty} - \frac{1}{\kappa_0}\right) \frac{n_q + 1/2 \pm 1/2}{|\mathbf{k} - \mathbf{k}'|^2} \delta(\epsilon'_k - \epsilon_k \pm \hbar\omega_{LO}). \tag{3.19}$$

3.3 Phonons In A Superlattice

The properties of phonons in a superlattice have attracted much attention in recent years and of the various physical properties of the semiconductor superlattice studied this has become one of the most interesting and controversial. Many different models have been proposed to calculate the phonon properties, ranging from simple linear chain models to full scale numerical calculations which include the coulomb forces between the ions. The many papers published and their widely differing conclusions have led to much confusion. A great deal of experimental work has also been performed, most of this has been measurements of Raman scattering. However the large amount of data collected has done little to clarify matters. In this section

a review of the literature is presented with emphasis on the derivation of a simple treatment of electron-LO phonon scattering in a superlattice.

A material with n atoms per unit cell has 3n branches in it's phonon dispersion relation. Since a superlattice can have a large unit cell containing many atoms, the superlattice phonon dispersion contains many branches. These branches are labeled either acoustic or optical depending on whether they lie in the acoustic or optical frequency region of the bulk materials of which the superlattice is composed (see fig 3.1). We begin by considering a $GaAs/GaAlAs$ superlattice. The acoustic phonon branches of bulk $GaAs$ and $GaAlAs$ overlap over a wide range of frequencies and thus the acoustic phonons of the superlattice are hardly affected by the superlattice structure and are well described by the elastic continuum model (Rytov 1956, Klein 1986). However the increased periodicity of the superlattice allows new phonon modes at the zone center of the Brillouin zone. In the continuum approximation the dispersion relation for acoustic phonons in a bulk material is given by the linear relation $\omega_q = v_s|\mathbf{q}|$. For a superlattice the acoustic phonon dispersion is approximately given by

$$\omega_q = v_{sL}|\mathbf{q} + \mathbf{G}| \tag{3.20}$$

where $\mathbf{G}$ are reciprocal lattice vectors with $\mathbf{G} = 2n\pi/l\ \hat{\mathbf{z}}$ in which n is an integer. Thus the new superlattice periodicity causes the original bulk acoustic phonon dispersion to be folded into the superlattice reduced Brillouin zone as shown in fig. 3.1. Due to this 'zone folding' some of the acoustic phonon modes become Raman active. One of the selection rules for Raman scattering is that

$$\mathbf{k}_S = \mathbf{k}_I + \mathbf{q} \tag{3.21}$$

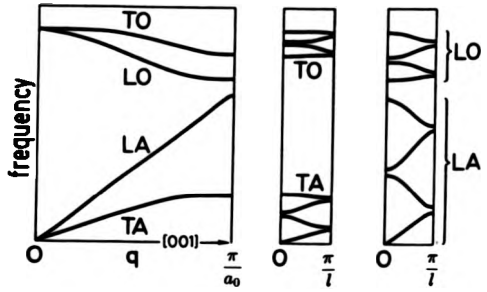

Figure 3.1: Zone folding of the phonon dispersion relation.

Schematic representation of the folding of the original bulk phonon dispersion into the superlattice reduced Brillouin zone.

where $\mathbf{k}_S, \mathbf{k}_I$ are the wavevectors of the scattered and incident light. Since the magnitude of the photon wavevector is given by $|\mathbf{k}| = \omega_k/c$ (where c is the speed of light) the photon wavevector is small and the condition to observe Raman scattering is

$$\mathbf{q} \cong 0. \tag{3.22}$$

In the backscattering configuration only the longitudinal modes are Raman active, and from (3.20) the predicted Raman frequency shift is given by

$$\omega = v_{SL}\, 2n\pi/l \tag{3.23}$$

and v_{SL} is an appropriate average of the velocities of sound of the constituent bulk materials. Experimental observations of Raman scattering by the longitudinal acoustic modes are in good agreement with the above result (Jusserand et al 1985).

Raman scattering by longitudinal optical (LO) modes has also been observed. The Raman spectra for a *GaAs/GaAlAs* superlattice was measured by Jusserand et al (1985), they found peaks in the Raman spectra with frequency shifts slightly lower than the LO phonon frequency of bulk *GaAs* at the Brillouin zone center. Unlike the case of the folded acoustic modes where the position of the peaks is a function of the superlattice periodic length (l), the position of the LO peaks seems to depend only on the width of the *GaAs* slab of the superlattice. The interpretation of this is as follows. Since the bulk LO branches of *GaAs* and *GaAlAs* only partially overlap there will be frequency regions where LO phonons propagate in bulk *GaAs* but not in bulk *GaAlAs*. Thus considering a *GaAs/GaAlAs* superlattice, in this frequency region the superlattice LO phonon vibrations are confined in the *GaAs* layer.

Many models have been proposed to study the optical phonon modes of a super-

lattice. While these all agree that the optical phonon modes are strongly affected by the superlattice structure there is considerable disparity between the predictions for the actual form of these modes. Many realistic calculations have also appeared they are however heavily numerical and intractable for transport calculations. Therefore it is desirable to use a simple model that can reproduce the essential features which are important for transport calculations. Simple linear chain models with nearest neighbor force constants have often, because of their simplicity, been used to calculate the superlattice phonon modes (Sawaki et al 1985, Fasolino et al 1986). However this model is only applicable when the phonon wavevector and atomic displacement are in the growth direction and the model does not properly include the Coulomb interaction between the ions. Thus this model is inappropriate for transport calculations and it's validity remains in doubt.

Simple models that are applicable when the phonon wavevector is in any direction have been based on macroscopic continuum models. The continuum models predict two types of modes. Guided modes where the optical displacement and electric field is entirely confined in slabs of one material type and the frequency of the guided modes is independent of the z component of the phonon wavevector. The other type of modes are called interface modes. These have optical displacement and scalar potential which are predicted by the continuum models to decay exponentially from the interfaces. By exploiting the periodicity of the superlattice the phonon optical displacement can be written as

$$\mathbf{W}_{LO}(\omega) = \mathbf{f}(z)\exp(i\mathbf{q}_{\parallel}.\mathbf{x}_{\parallel}) \qquad (3.24)$$

where

$$\mathbf{f}(z+nl) = \mathbf{f}(z)\exp(iQnl) \tag{3.25}$$

with $\mathbf{q}_{\parallel} = (q_x, q_y, 0), \mathbf{x}_{\parallel} = (x, y, 0)$ and the superlattice phonon wavevector $\mathbf{q}^{SL} = (q_x, q_y, Q)$. The usual approach to the continuum model is to assume that in any slab $\mathbf{f}(z)$ is of the form

$$\begin{aligned} \mathbf{f}(z) &= \mathbf{A}\exp(iq_z z) + \mathbf{B}\exp(-iq_z z) \\ \nabla \times [\mathbf{f}(z)\exp(i\mathbf{q}_{\parallel}.\mathbf{x}_{\parallel})] &= 0 \end{aligned} \tag{3.26}$$

where q_z can be real or imaginary. Then at a frequency ω such that LO modes propagate in *GaAs* but not in *AlAs*, $\mathbf{f}(z)$ is made up of traveling plane waves in *GaAs* and exponentially decaying waves in *AlAs*.

$$\mathbf{f}(z) = \begin{cases} \hat{\xi}(q_z)A\exp(iq_z z) + \hat{\xi}(-q_z)B\exp(-iq_z z) & GaAs \quad -a < z < a \\ \hat{\xi}(-i\lambda)C\exp(\lambda z) + \hat{\xi}(i\lambda)C\exp(-\lambda z) & AlAs \quad a < z < a+2b \end{cases} \tag{3.27}$$

where

$$\xi(k_z) = \mathbf{q}_{\parallel} + k_z\hat{\mathbf{z}}. \tag{3.28}$$

The coefficients (A,B,C,D, q_z and λ) in (3.27) are determined by applying appropriate boundary conditions at the interface. However there has been considerable controversy as to what the correct boundary conditions are. The dielectric continuum model (DCM) uses the Born and Huang equations (3.5) and applies standard electrostatic boundary conditions at the interfaces. Fuchs and Kliewer guided modes are obtained (Fuchs and Kliewer 1965), see fig. 3.2. Others have suggested that $\mathbf{W}_z$ (the optical displacement in the growth direction) should have nodes at the interface (Ridley 1989, Cardona 1989) and this gives results similar to the hydrodynamic continuum model (Babiker 1986). Simple linear chain models also predict that W_z

has nodes at the interface. The results for the two continuum models are completely different (fig 3.2) with the DCM predicting guided modes with anti-nodes in W_z and the hydrodynamic continuum model predicting guided modes with anti-nodes in $W_\parallel$ (the optical displacement in the direction parallel to the slabs) at the interfaces. Both continuum models also predict interface modes where the displacement is maximum at the interfaces and decays exponentially into the slabs. However the two models are in poor agreement as regards the properties of the interface modes, and in particular the frequency dependence e.g. compare fig. 2b in Fuchs and Kliewer (1965) with fig. 5 in Babiker (1986). It is therefore necessary to compare the predictions of the two continuum models with experimental data and realistic microscopic calculations to deduce whether either of the continuum models can give a good description of electron-LO phonon scattering in a superlattice.

Realistic microscopic models suggest that in a *GaAs/AlAs* superlattice both $W_\parallel$ and W_z have nodes at the interface (Richter et al 1987, Ren et al 1988, Huang et al 1988, Tsuchiya et al 1989). Thus neither of the continuum models seems to give a correct description of the optical displacement. However it is not the optical displacement which is of interest for transport calculations, the important quantity is the scalar potential associated with the optical modes. Unfortunately most of the calculations involving realistic microscopic models do not give any results for the form of the scalar potential. However Huang et al (1988) have made a comparison of the scalar potentials obtained with their microscopic model and the DCM. They find that the scalar potential associated with both the guided and interface modes is well described by the DCM (fig. 3.3). The dispersion curve of the DCM interface modes is also in good agreement with realistic microscopic models (fig 3.4). We

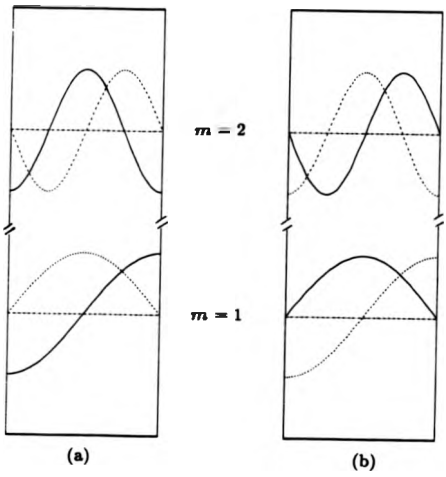

Figure 3.2: The predicted ionic displacement for the guided modes of the two continuum models.

The two continuum models give very different results for $W_{\parallel}$ (Solid line) and W_{s} (dashed line). a: hydrodynamic continuum model, b: DCM.

show in appendix B how the DCM can be modified to give a correct description of the optical displacement as well as the scalar potential.

Comparison with experiment is limited since Raman scattering data can usually only give the frequency of the optical phonon modes when $\mathbf{q} \simeq 0$. The DCM predicts that all the LO guided modes confined in *GaAs* oscillate at the same frequency ω_{LO}^{GaAs}. This is because the Born and Huang equations ignore the spatial dispersion of the bulk optical modes ie. assume $\omega_{LO}^{GaAs}(\mathbf{q}^{bulk})$ is independent of $\mathbf{q}^{bulk}$. The hydrodynamic continuum model does include spatial dispersion, and the bulk LO dispersion relation is written as

$$\omega_{LO}^2(\mathbf{q}^{bulk}) = \omega_{LO}^2 - \beta|\mathbf{q}^{bulk}|^2 \tag{3.29}$$

where β is a parameter fitted to the bulk dispersion curve. The frequency of the superlattice LO guided modes is then given by

$$\omega_{LO}^2(\mathbf{q}^{SL}) = \omega_{LO}^2 - \beta(q_x^2 + q_y^2 + q_z^2) \tag{3.30}$$

where $\mathbf{q}^{SL} = (q_x, q_y, Q)$ and the hydrodynamic model predicts that

$$q_z = \frac{m\pi}{2a} \tag{3.31}$$

for the m_{th} guided mode. Thus the hydrodynamic model predicts that the Raman frequency shift is given by

$$\omega^2 = \omega_{LO}^2 - \beta\left(\frac{m\pi}{2a}\right)^2. \tag{3.32}$$

The above equation is in reasonable agreement with experiment. However it is worth pointing out that the DCM also predicts that $q_z = m\pi/2a$ thus if spatial dispersion were included in the DCM the two continuum models would give the same results

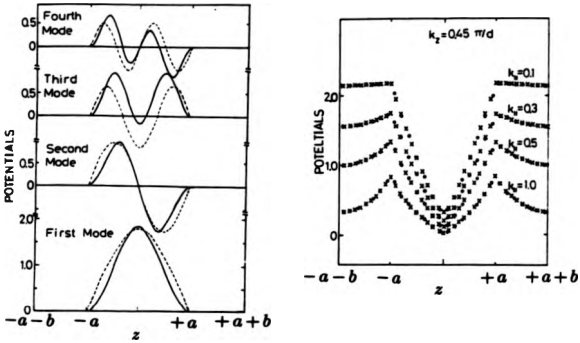

Figure 3.3: Comparison of the DCM with a realistic microscopic model. Huang et al (1988) make a comparison of the scalar potential associated the optical modes of the DCM with their microscopic model in the limit of vanishing bulk phonon dispersion. The figure on left gives a comparison of the guided modes. Solid line: microscopic model, dashed line: DCM. The figure on right is a comparison of the modulus of the potential for interface modes. Dots: microscopic model, crosses: DCM. Figure reproduced from Huang and Zhu (1988).

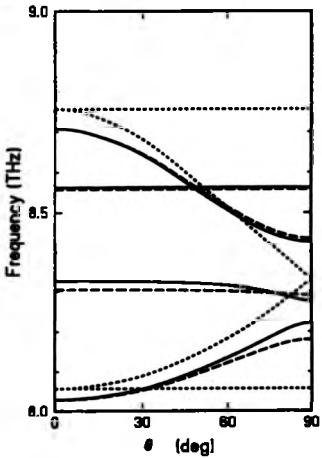

Figure 3.4: Frequency dependence of superlattice phonon modes.

The frequency dependence of the phonon modes on the wave-vector (q^{SL}) direction when $q^{SL} \rightarrow 0$. The direction of q^{SL} is given by the angle θ, where $\theta = 0^o$ corresponds to q^{SL} pointing in the growth direction and $\theta = 90^o$ corresponds to the direction parallel to the layers. The two curves with a strong dependence on θ correspond to the interface modes. The guided modes have frequency independent of θ. The results for the DCM (dotted curve) and the the microscopic model (solid curve) are seen to be in good agreement. Figure reproduced from Tsuchiya et al 1989.

for the frequencies of the guided modes. Raman scattering by the interface modes is more conclusive, there is considerable evidence for Raman scattering by the DCM interface modes (Sood et al 1985a, Nakayama et al 1988). While the interface modes of the hydrodynamic continuum model have not been observed.

Sood et al (1985b) uses Raman scattering selection rules (see Cardona 1989) to deduce the symmetry of the scalar potential and $\mathbf{W}_s$ of the *GaAs/AlAs* superlattice phonons. In non-resonant Raman scattering the phonons couple to the incident and scattered light via the deformation potential. For back scattering in the growth direction Raman scattering is by superlattice LO modes which have $\mathbf{W}_s$ with even symmetry within a slab. In resonant Raman scattering the energy of an incident photon of light is set very close to the energy of the first exciton state of the superlattice. The phonon-exciton interaction is via the Frohlich mechanism and thus only phonon modes which have symmetric scalar potential in the *GaAs* slabs are observed. It is worth pointing out that for resonant Raman scattering conservation of crystal momentum (3.21) is not obeyed. Sood et al (1985a) discuss the possible causes for this. From their results Sood et al (1985b) deduce that LO1, LO3 and LO5 have symmetric $\mathbf{W}_s$ and anti-symmetric scalar potential while LO2, LO4 and LO6 have anti-symmetric $\mathbf{W}_s$ and symmetric scalar potential. Where LO1, LO2 etc are mode labels for modes with frequency between ω_{LO}^{GaAs} and ω_{TO}^{GaAs} with LO1 having the highest frequency and LO6 the lowest. They then assume that LO1 corresponded to the first guided mode (m=1), LO2 to the second guided mode (m=2) etc. . If this mode assignment is used the results are in good agreement with the hydrodynamic continuum model and this work has been used in support of that model. However we show that this mode assignment is not unambiguous and that

it is possible to reinterpret the data as supporting the DCM. If we look at fig 3.4 we see that the highest frequency mode is not a guided mode but an interface mode, thus we may interpret LO1 as an interface mode. Then LO2 is the first guided mode (m=1), LO3 the second guided mode etc. In the light of this reinterpretation the results of Sood at al (1985b) are now in agreement with the DCM. Curiously Sood et al did assign one of the Raman peaks to the interface mode oscillating near ω_{TO}^{GaAs}. However none of the Raman peaks were assigned to the interface mode oscillating near ω_{LO}^{GaAs}, this mode should be observed in non-resonant Raman scattering (since it has symmetric $\mathbf{W}_1$ in the *GaAs* slabs) and thus LO1 should be interpreted as an interface mode.

3.4 Dielectric Continuum Model

Although there is still much controversy over the correct form of the optical phonon modes in a superlattice, there seems to be considerable evidence that the use of the DCM can give a correct treatment of electron -LO phonon scattering in a superlattice. We therefore use the DCM to calculate the LO phonon modes in a *GaAs/GaAlAs* superlattice.

An alloy material such as bulk *GaAlAs* has two LO modes and two TO modes (Baroni et al 1990, Kim et al 1979). One of the LO modes oscillates with a frequency close to ω_{LO}^{GaAs} and corresponds to vibrations of the Ga cations. The other LO mode oscillates near ω_{LO}^{AlAs} and corresponds to vibrations of the Al cations. It is not clear how to include this property of *GaAlAs* into the DCM, consequently to proceed further we ignore the AlAs like LO and TO modes and consider only the

GaAs like LO and TO modes of *GaAlAs*. An additional feature is that the LO phonon branches of bulk *GaAs* and *GaAlAs* overlap partially, in the DCM this fact is not taken into account since spatial dispersion is ignored and the LO branches are assumed to be flat. However we can still have confidence in the DCM as the superlattice modes of most significance for transport calculations have frequencies in the region where the bulk LO branches do not overlap.

To calculate the scalar potential associated with the optical phonon modes we begin by writing down Maxwell's equations in the absence of free charges and neglecting retardation effects

$$\nabla \times \mathbf{E} = 0 \ , \ \nabla . \mathbf{D} = 0. \tag{3.33}$$

These equations are satisfied when

$$\kappa_i(\omega_q)\nabla^2 \nu_q(\mathbf{r}) = 0 \tag{3.34}$$

where $\nu_q(\mathbf{r})$ is the scalar potential and the superlattice periodicity implies that it must be of the form

$$\nu_q(\mathbf{r}) = \exp(i\mathbf{q}_\parallel . \mathbf{x}_\parallel)\Phi(z) \tag{3.35}$$

with

$$\Phi(z + nl) = \Phi(z)\exp(iQnl). \tag{3.36}$$

Solutions for guided modes confined in *GaAs* occur when $\kappa^{GaAs}(\omega_q) = 0$, i.e. when $\omega_q = \omega_{LO}^{GaAs}$. Thus, writing $\Phi(z) = \Phi_G(z)$ we have

$$\Phi_G(z) = \begin{cases} \left.\begin{array}{ll} A_G \cos(m\pi z/2a) & m = 1,3,5\ldots \\ A_G \sin(m\pi z/2a) & m = 2,4,6\ldots \end{array}\right\} & GaAs \quad -a < z < a \\ 0 & GaAlAs \quad -a - 2b < z < -a \end{cases} \tag{3.37}$$

For the interface modes $\nabla^2\nu_\phi(\mathbf{r}) = 0$ and writing $\Phi(z) = \Phi_I(z)$ we have

$$\Phi_I(z) = \begin{cases} A_I \exp(q_\parallel z) + B_I \exp(-q_\parallel z) & -a < z < a \\ C_I \exp(q_\parallel z) + D_I \exp(-q_\parallel z) & -a-2b < z < -a \end{cases} \tag{3.38}$$

The coefficients A_I, B_I, C_I, D_I are obtained by applying the electrostatic boundary conditions that $\mathbf{E}_\parallel$ and $\mathbf{D}_z$ are continuous at an interface. Here $\mathbf{E}_\parallel$ is the component of the electric field parallel to the interface and $\mathbf{D}_z$ is the component of Maxwell's displacement vector in the growth direction. The above conditions are satisfied when $\Phi(z)$ and $\kappa_z(\omega_\phi)\partial\Phi/\partial z$ are continuous at an interface. Applying the boundary conditions the following equations are obtained

$$\begin{aligned} A_I f_1^{-1} + B_I f_1 &= C_I f_1^{-1} + D_I f_1 \\ A_I f_1 + B_I f_1^{-1} &= [C_I f_2 + D_I f_2^{-1}]\exp(iQl) \\ \kappa^{GaAs}(\omega_\phi)[A_I f_1^{-1} - B_I f_1] &= \kappa^{GaAlAs}(\omega_\phi)[C_I f_1^{-1} - D_I f_1] \\ \kappa^{GaAs}(\omega_\phi)[A_I f_1 - B_I f_1^{-1}] &= \kappa^{GaAlAs}(\omega_\phi)[C_I f_2 - D_I f_2^{-1}]\exp(iQl) \end{aligned} \tag{3.39}$$

where $f_1 = \exp(q_\parallel a)$ and $f_2 = \exp[q_\parallel(a-l)]$. Non trivial solutions are obtained when the following dispersion relation is satisfied :

$$\frac{1}{2}(\gamma + \gamma^{-1})\sinh(2q_\parallel b)\sinh(2q_\parallel a) + \cosh(2q_\parallel b)\cosh(2q_\parallel a) = \cos(Ql). \tag{3.40}$$

With $\gamma = \kappa^{GaAs}(\omega_\phi)/\kappa^{GaAlAs}(\omega_\phi)$. There are four interface modes and in the limit $q_\parallel \to 0$ they approach the bulk LO and TO frequencies $\omega_{LO}^{GaAs}, \omega_{TO}^{GaAs}, \omega_{LO}^{AlGaAs}$ and ω_{TO}^{GaAlAs}. The normal modes are given in terms of the scalar potential by

$$\mathbf{W}_\phi(\mathbf{r}) = c_i(-\nabla\nu_\phi(\mathbf{r})) \tag{3.41}$$

where c_i is material dependent and is given by the Born and Huang equations (3.5):

$$c_i(\omega_\phi) = \omega_{TO,i}[\epsilon_0(\kappa_{0,i} - \kappa_{\infty,i})]^{1/2}[\rho_{r,i}(\omega_\phi^2 - \omega_{TO,i}^2)]^{-1/2}. \tag{3.42}$$

The subscript s refers to either *GaAs* or *GaAlAs*. To ensure that $\mathbf{W}_q(\mathbf{r})$ is normalized

$$\int |\mathbf{W}_q(\mathbf{r})|^2 \, dV = 1 \tag{3.43}$$

the following condition is imposed on $\Phi(z)$,

$$\int_{-2b-a}^{+a} \left\{ q_\parallel^2 |\Phi(z)|^2 + \left| \frac{\partial \Phi}{\partial z} \right|^2 \right\} \epsilon_i^2(\omega_q) \, dz = \frac{l}{V}. \tag{3.44}$$

The total ionic displacement is written in terms of the normal modes as (Bruesch 1982)

$$\mathbf{W}(\mathbf{r}) = \sum_q \left(\frac{\hbar}{2\omega_q \rho_{r,s}} \right)^{1/2} (b_{-q}^+ + b_q) \mathbf{W}_q(\mathbf{r}) \tag{3.45}$$

and thus the total scalar potential

$$\nu(\mathbf{r}) = \sum_q \left(\frac{\hbar}{2\omega_q \rho_{r,s}} \right)^{1/2} (b_{-q}^+ + b_q) \Phi(z) \exp(i\mathbf{q}_\parallel . \mathbf{x}_\parallel). \tag{3.46}$$

Having obtained the scalar potential the scattering rates can then be calculated using Fermi's golden rule. For the guided modes the intra-band scattering rate is given by

$$\begin{aligned} T_G(\mathbf{k}, \mathbf{k}') \; &= \frac{l}{a} \alpha \left[(\mathbf{k}_\parallel - \mathbf{k}'_\parallel)^2 + \left(\frac{m\pi}{2a} \right)^2 \right]^{-1} \left| \int_{-a}^{+a} \cos \frac{m\pi z}{2a} \phi^2(z) \, dz \right|^2 \\ &\quad \times \delta(\epsilon_{\mathbf{k}'} - \epsilon_{\mathbf{k}} \pm \hbar\omega_{LO}^{GaAs}) \end{aligned} \tag{3.47}$$

where $m = 1, 3, 5....$ For cases considered here the $(m\pi/2a)$ term is much bigger than the $|\mathbf{k}_\parallel - \mathbf{k}'_\parallel|$ term, consequently scattering by guided modes is approximately proportional to $(a/m)^2$. The even m guided modes do not contribute to the intra-band scattering rate since they have a scalar potential which is anti-symmetric within the *GaAs* slabs. As can be seen from the above equation the $m = 1$ guided mode scatters electrons more strongly than the $m = 3$ guided mode. We find that scattering from the $m = 1$ guided mode is an order of magnitude larger than

scattering from the $m = 3$ guided mode. For the interface modes the scattering rate is given by

$$T_I(\mathbf{k},\mathbf{k}') = \frac{l}{4}\alpha\frac{\omega_{LO}^{GaAs}}{\omega_q}\left(\frac{c_{GaAs}(\omega_{LO}^{GaAs})}{c_{GaAlAs}(\omega_q)}\right)^2\left|\int_{-a-2b}^{+a}\frac{\Phi_I(z)}{A_I}\phi^2(z)\left(\frac{\rho_{r,GaAs}}{\rho_{r,i}}\right)^{1/2}dz\right|^2$$

$$\times\left[q_\parallel\left\{\left(\frac{c_{GaAs}(\omega_q)}{c_{GaAlAs}(\omega_q)}\right)^2\sinh(2q_\parallel a)+\left|\frac{D_I}{A_I}\right|^2\exp(q_\parallel l)\sinh(2q_\parallel b)\right\}\right]^{-1}$$

$$\times\,\delta_{k'_\parallel-k_\parallel-q_\parallel}\,\delta_{k'_z-k_z,Q}\,\delta(\epsilon_{k'}-\epsilon_k\pm\hbar\omega_q) \tag{3.48}$$

where ω_q is the frequency for the interface mode and

$$\alpha = \frac{\pi e^2\omega_{LO}^{GaAs}}{V\epsilon_0}\left(\frac{1}{\kappa_\infty^{GaAs}}-\frac{1}{\kappa_0^{GaAs}}\right)(n_q+\frac{1}{2}\pm\frac{1}{2}). \tag{3.49}$$

Of the four interface modes, the two with frequencies near the bulk TO frequencies ω_{TO}^{GaAs} and ω_{TO}^{GaAlAs} hardly contribute to the scattering since only a weak scalar potential is associated with these modes i.e. $c_i(\omega_{TO}^i)\to\infty$. The interface mode whose frequency is near ω_{LO}^{GaAlAs} dominates the scattering since it has a scalar potential which is approximately symmetric within the $GaAs$ slabs. The interface mode which has frequency near ω_{LO}^{GaAs} has scalar potential which is approximately anti-symmetric in the $GaAs$ slabs. We use these results to calculate the optical phonon limited mobility in the next chapter.

3.5 Interface Roughness scattering

A scattering mechanism which is not present in bulk materials but which has been shown to be important in superlattices and heterostructures is interface roughness (IFR) scattering. The interface between a $GaAs$ and a $GaAlAs$ layer is not perfectly

smooth but contains asperities which scatter the electrons. While extensive studies of IFR scattering in Si metal-oxide-semiconductor inversion layers have been carried out (Ando, Fowler and Stern 1982) very little work has been done on IFR scattering in $GaAs/GaAlAs$ structures. One reason for this is that an early calculations of IFR scattering in a $GaAs/GaAlAs$ heterostructure assumed the form of the IFR of a $GaAs/GaAlAs$ interface to be the same as that for a Si/SiO_2 interface and thus concluded that IFR scattering is unimportant in $GaAs/GaAlAs$ structures (Ando 1982). However recent work shows that IFR scattering is indeed important and can dominate the scattering in $GaAs/GaAlAs$ structures. Sakaki et al (1987) found a L_W^6 dependence for the electron mobility in $GaAs/AlAs$ quantum wells (L_W is the width of the $GaAs$ layer) which is characteristic of IFR scattering.

The IFR scattering is studied within a simple model (Prange and Nee 1968). The IFR is assumed to be small and slowly varying and to be characterised by a height Ω and a lateral size Λ. For a Si/SiO_2 interface, the IFR parameters are usually determined by fitting the calculated IFR limited mobility to the experimentally measured mobility. Ando (1977) determines the parameters to be of the order of $\Omega = 4.3$ Å and $\Lambda = 15$ Å. However for a $GaAs/GaAlAs$ interface the IFR parameter Λ is of the order of a 100 Å. To calculate the IFR scattering it is necessary to derive the scattering potential H_{SR} due to the IFR and this is obtained by using the effective mass theorem. Experimental evidence shows that the form of the IFR of $GaAlAs$ grown on a $GaAs$ surface can be different from that of $GaAs$ on $GaAlAs$ (Joyce et al 1986). Thus we treat scattering from the two types of interfaces separately, and use the subscript $i = 1$ for $GaAs$ grown on $GaAlAs$ and the subscript $i = 2$ for $GaAlAs$ on $GaAs$. If the deviation of the interface at $z = nl + a$ (

GaAs grown on *GaAlAs*) from a flat plane is given by $\Omega_1^n(x,y)$ then it's scattering potential for the IFR is

$$H_{1,SR}^n = \begin{cases} V_0 & nl+a+\Omega_1^n(x,y) < z < nl+a \quad \Omega_1^n(x,y) < 0 \\ -V_0 & nl+a < z < nl+a+\Omega_1^n(x,y) \quad \Omega_1^n(x,y) > 0 \\ 0 & otherwise \end{cases} \tag{3.50}$$

where V_0 is the barrier potential height and SR means surface roughness. The deviation of the interface at $z = nl - a$ (*GaAlAs* grown on *GaAs*) from a flat plane is given by $\Omega_2^n(x,y)$, and its scattering potential $H_{2,SR}^n$ is written in a similar manner to $H_{1,SR}^n$. The total scattering potential, including the contribution from all the interfaces is given by

$$H_{SR} = \sum_{i=1}^{2} \sum_n H_{i,SR}^n. \tag{3.51}$$

Ando, Fowler and Stern (1982) include an additional term in their scattering potential which is produced by the change in the electron density distribution due to the IFR. However since we are assuming low doping levels this term should be negligible in the present case.

Although there is no definite physical grounds for doing so, it is usually assumed that the correlation of the IFR has a Gaussian form

$$< \Omega_i^n(x,y)\Omega_j^m(x',y') >= \delta_{n,m}\delta_{i,j}\Omega_i^2 \exp[-\Lambda_i^{-2}(\mathbf{x}_\parallel - \mathbf{x}'_\parallel)^2]. \tag{3.52}$$

Using this auto-correlation function and assuming that the electron envelope function is almost constant near the interface, the scattering matrix element is found to be

$$|< \mathbf{k}|H_{SR}|\mathbf{k}' >|^2 = \pi \frac{l}{V} V_0^2 \phi^4(a) \sum_{i=1}^{2} \Omega_i^2 \Lambda_i^2 \exp\left(-\frac{\Lambda_i^2}{4}(\mathbf{k}'_\parallel - \mathbf{k}_\parallel)^2\right). \tag{3.53}$$

In deriving the above equation, inter-well scattering has been ignored i.e. we make use of (1.5). The scattering rate is then given as

$$T(\mathbf{k},\mathbf{k}') = \frac{2\pi^2 l}{\hbar V} V_0^2 \phi^4(a) \sum_{i=1}^{2} \Omega_i^2 \Lambda_i^2 \exp\left(-\frac{\Lambda_i^2}{4}(\mathbf{k}_\parallel' - \mathbf{k}_\parallel)^2\right) \delta(\epsilon - \epsilon'). \tag{3.54}$$

The reciprocal of the electron lifetime is then given by

$$\tau^{-1}(\mathbf{k}) = \frac{V}{8\pi^3} \int T(\mathbf{k},\mathbf{k}')\, d^3\mathbf{k}'$$

$$= \frac{l}{4\pi\hbar} V_0^2 \phi^4(a) \sum_{i=1}^{2} \Omega_i^2 \Lambda_i^2 \int_{-\pi/l}^{\pi/l} dk_z' \int \exp\left(-\frac{\Lambda_i^2}{4}(\mathbf{k}_\parallel' - \mathbf{k}_\parallel)^2\right) \delta(\epsilon - \epsilon')\, d^2\mathbf{k}_\parallel'. \tag{3.55}$$

In contrast with previous studies of IFR scattering we have not taken the barrier height V_0 to be infinite. While the approximation of infinite barrier height is adequate for Si MOSFETs and $GaAs/AlAs$ heterostructures, we find it leads to large errors in a $GaAs/Ga_{0.7}Al_{0.3}As$ system where the barrier height is only 250 meV. In appendix A we show

$$\phi(a) = \left(\frac{\hbar^2}{2m^*(V_0 - E_0)}\right)^{1/2} \left.\frac{d\phi}{dz}\right|_{z=a} \tag{3.56}$$

where E_0 is the lowest energy level of a finite potential well of width 2a and barrier height V_0. Hence

$$V_0^2 \phi^4(a) = \frac{\hbar^4 V_0^2}{4m^{*2}(V_0 - E_0)^2} A^4 k_0^4 \sin^4 k_0 a. \tag{3.57}$$

For an infinite barrier height $A = a^{-1/2}$ and $k_0 a = \pi/2$. We can see why the infinite barrier approximation leads to large errors by taking an example: a finite well of width 30 Å and a barrier height 250 meV. In this case $E_0 = 137meV$ and the gradient of $\phi(z)$ at $z = a$ is one quarter of that predicted for an infinite potential well. Since, in the IFR scattering rate, the gradient is taken to the fourth power

this difference is considerably magnified. Consequently the use of the infinite barrier height approximation would overestimate the scattering by two orders of magnitude. As the well width is increased this error is reduced. For a well of width 50 Å assuming an infinite barrier height would overestimate the scattering by one order of magnitude. These conclusions have also been reached independently by Wataya et al (1989). However it is still interesting to see what the form of the IFR scattering rate is in the infinite barrier approximation. Thus, if we take the limit $V_0 \rightarrow \infty$ (the miniband width $2\Delta \rightarrow 0$),

$$\lim_{V_0 \rightarrow \infty} \tau^{-1}(\mathbf{k}) = \frac{\pi^4 \hbar^3}{2(m^*)^2(2a)^6} \sum_{i=1}^{2} \Omega_i^2 \Lambda_i^2 \int \exp\left(-\frac{\Lambda_i^2}{4}(\mathbf{k}'_{\parallel} - \mathbf{k}_{\parallel})^2\right) \delta(\epsilon - \epsilon')\, d^2\mathbf{k}'_{\parallel}. \quad (3.58)$$

From the above equation we see that in the infinite barrier approximation the electron lifetime is proportional to $(2a)^6$ where $2a$ is the width of a $GaAs$ layer in the superlattice.

Some studies of IFR scattering use as the scattering potential, the fluctuations in the lowest energy level of an infinite potential well due to variations in the well width (Sakaki et al 1987). Proceeding similarly we may write

$$H_{SR} = \frac{\partial E_0}{\partial L_W}[\Omega_1(x,y) - \Omega_2(x,y)]. \quad (3.59)$$

E_0 is the lowest energy level for the infinite potential well of width L_W and $\Omega_1(x,y) - \Omega_2(x,y)$ is the change in the well width due to the IFR. Making use of the autocorrelation function, the scattering rate for quasi-2D electrons in an xy plane of area A is

$$T(\mathbf{k}_{\parallel}, \mathbf{k}'_{\parallel}) = \frac{2\pi^6 \hbar^3}{A(m^*)^2 L_W^6} \sum_{i=1}^{2} \Omega_i^2 \Lambda_i^2 \exp\left(-\frac{\Lambda_i^2}{4}(\mathbf{k}'_{\parallel} - \mathbf{k}_{\parallel})^2\right) \delta(\epsilon - \epsilon'). \quad (3.60)$$

We see that in this case the scattering rate is proportional to to L_W^6. This means that the IFR scattering rate is much more important for narrow wells and that

the mobility of an infinite potential well is proportional to L_W^6. In this case the reciprocal of the electron lifetime can now be calculated as

$$\begin{aligned}\tau^{-1}(\mathbf{k}) &= \frac{A}{4\pi^2}\int T(\mathbf{k}_\parallel,\mathbf{k}'_\parallel)\,d^2\mathbf{k}'_\parallel \\ &= \frac{\pi^4\hbar^3}{2(m^*)^2L_W^6}\sum_{i=1}^{2}\Omega_i^2\Lambda_i^2\int \exp\left(-\frac{\Lambda_i^2}{4}(\mathbf{k}'_\parallel-\mathbf{k}_\parallel)^2\right)\delta(\epsilon-\epsilon')\,d^2\mathbf{k}'_\parallel.\end{aligned} \tag{3.61}$$

This equation is identical to (3.58) reproducing the L_W^{-6} dependence. Thus in the limit of infinite barrier height, the two scattering potentials (3.51) and (3.59) are equivalent.

Chapter 4

Mobility Calculations

Once the superlattice miniband structure and the scattering rates have been calculated , it is then possible to calculate the superlattice transport properties. Since the superlattice mini-band structure is highly anisotropic the transport properties can be separated into two distinct cases. When the electric field is applied parallel to the superlattice layers we have parallel transport. However the more interesting case is when the electric field is applied perpendicular to the superlattice layers, this is called vertical transport.

4.1 Vertical Transport

Interest in superlattices arose from the possibility , when the electric field is applied perpendicular to the superlattice layers, of observing negative differential resistance and Bloch oscillations (Esaki and Tsu 1970). Thus interest in vertical transport has always received much more attention than parallel transport.

There are two fundamentally different approaches to the treatment of vertical

transport. If the disorder in a superlattice is sufficiently strong then the electron states become localized in the growth direction. The electron transport is then via the LO phonon assisted hopping of the electrons through the barriers. This approach to the electron transport is suitable for *GaAs/GaAlAs* superlattices with wide barrier (*GaAlAs*) layers and therefore a small miniband width. Calecki et al (1984) have already given a treatment of this hopping transport. Although the effect of the superlattice structure on the LO phonon modes was ignored by Calecki et al (1984) and the bulk LO phonon-electron scattering rate (3.19) assumed their treatment is adequate since for superlattices with wide layers the superlattice LO phonon scattering rate (3.47,3.48) approaches the value of the bulk LO phonon scattering rate (3.19).

If the electrons have extended Bloch states the transport can be described by the Boltzmann transport equation. There is considerable experimental evidence that for superlattice with narrow enough barrier layers electron transport is by extended Bloch states (Duffield et al 1986, Deveaud et al 1988, England et al 1989, Sibille et al 1987) and in this section we calculate the superlattice transport properties using the Boltzmann transport equation. As yet a more general approach that combines both approaches and examines the crossover from Bloch to hopping transport has not been carried out. However the crossover from Bloch to hopping transport has been experimentally observed (Sibille et al 1987).

4.1.1 Polar Optical Phonon Scattering

Electron-LO phonon scattering is the dominant scattering mechanism in bulk GaAs at room temperature, it may thus be expected to be important in a *GaAs/GaAlAs*

superlattice. Palmier and Chomette (1982) have already made a study of the LO phonon limited mobility in a *GaAs/GaAlAs* superlattice. However they assumed the bulk LO phonon scattering rate (3.19) and assumed that the relaxation time for LO phonon scattering was equal to to electron lifetime, which is incorrect. For LO phonon scattering ,which is an inelastic scattering mechanism, no simple formula for the relaxation time exists. Warren and Butcher(1986) improved the calculations of Palmier and Chomette (1982) and used an iterative method to calculate the LO phonon limited mobility. This was found to result in an increase in the predicted mobility by up to a factor of two. But it is well known that the optical phonon modes in a superlattice are strongly perturbed by the superlattice structure and become mostly confined to layers of one material type. There is considerable evidence from measurements of energy relaxation times in multiple quantum well (MQW) systems that the electron-LO phonon scattering rate is significantly reduced in these structures. Therefore we recalculate the LO phonon limited mobility including the effect of the superlattice structure on the phonon modes and using the correct scattering rates (3.47,3.48).

The experimentally measured energy relaxation time for electrons in (MQW) systems have been found to significantly larger than in bulk materials. The predicted energy relaxation time for electrons in bulk *GaAs* is approximately 0.15 ps while Ryan et al (1984) measured the electron energy relaxation time in a *GaAs/GaAlAs* MQW to be 7ps. Since LO phonon scattering is the dominant mechanism by which hot electrons lose energy in bulk *GaAs*, the measurement of the anomalously long energy relaxation time in *GaAs/GaAlAs* MQW has led to speculation that this may be due to a reduction of the electron-LO phonon scattering rate. This has conse-

quently led to considerable interest in the form the superlattice optical modes and the effect of the 'confinement' of the optical modes on the scattering rates. A discussion of energy relaxation in *GaAs/GaAlAs* MQW is given by Ryan(1986). Jain and Das Sarma(1989) calculate the energy relaxation time for electrons scattered from the first excited miniband to the lowest miniband ($2 \rightarrow 1$) in a 50 Å *GaAs/GaAlAs* quantum well (QW) using the phonon modes of the DCM. For a quantum well of width 50 Å with barrier height of 250 mev they calculate the energy relaxation time $\tau_{21} = 10.5ps$. This result is in good agreement with experimental results (Seilmeier et al 1988). A calculation assuming bulk LO phonon modes would underestimate τ_{21} by an order of magnitude. Tatham et al (1989) measured the energy relaxation time in a *GaAs/GaAlAs* MQW with the *GaAs* slabs of width 146 Å. They measured an upper limit of 1ps for τ_{21} and compared it with their theoretical calculations. Using the DCM model they calculated τ_{21} to be 630 fs and for Babiker's hydrodynamic continuum model (Babiker 1986) they calculated τ_{21} to be 360 fs. These experiments show the strong dependence of the electron-LO phonon scattering rate on the *GaAs* well widths and, as would be expected, the 'confinement' of the optical phonon modes is more important for systems with narrow layers of *GaAs*. It has been proposed that the presence of a non-equilibrium hot phonon population can also significantly increase the energy relaxation time, however this is only important for intraband scattering (Jain and Das Sarma 1989).

To calculate the LO phonon limited mobility we consider the application of a small electric field to the superlattice perpendicular to the layers. The electron distribution can then be written as

$$f = f_0 + g \tag{4.1}$$

where f_0 is the Fermi-Dirac distribution function and g is the first order perturbation. From the linearised Boltzmann transport equation, assuming non-degenerate statistics i.e. $f_0 << 1$, we have

$$g(\mathbf{k}) = \tau(\mathbf{k}) \int g(\mathbf{k}') P(\mathbf{k}', \mathbf{k})\, d^3\mathbf{k}' + \frac{e}{\hbar} E_z \frac{df_0}{dk_z} \tag{4.2}$$

where $P(\mathbf{k}, \mathbf{k}') = (V/8\pi^3) T(\mathbf{k}.\mathbf{k}')$ and

$$\tau(\mathbf{k}) = \left(\int P(\mathbf{k}, \mathbf{k}')\, d^3\mathbf{k}' \right)^{-1} \tag{4.3}$$

is the lifetime of the electron state $\mathbf{k}$. The LO phonon limited electron lifetimes all have a similar form. For electrons with energy less than $\hbar\omega_{LO}$ the electrons can only absorb phonons and this process is proportional to n_q. Once the energy of the electrons is above $\hbar\omega_{LO}$ the electrons can also emit phonons and this process is proportional $(n_q + 1)$, consequently the electron lifetime begins to fall rapidly. Between $\hbar\omega_{LO}$ and $2\Delta + \hbar\omega_{LO}$ the electron lifetime continues to fall as the density of final states the electrons can scatter into increases. Above $\hbar\omega_{LO}$ the electron lifetime increases as the electrons LO phonon scattering involves phonons with larger wavevectors.

To calculate the first order perturbation of the electron distribution function an iterative procedure is used. Beginning with an initial guess $g_0(\mathbf{k}) = 0$ which is substituted into (4.2) to obtain $g_1(\mathbf{k})$ and so on. Convergence is fairly rapid and we find that five iterations are needed to obtain a reasonable accuracy. Once the perturbed distribution function has been calculated the determination of the mobility is a simple matter. The results are given in fig 4.1 , for comparison the results when bulk phonon scattering (3.17) is assumed are also shown. The reader should note that Warren et al (1986) (who also calculated mobility in a superlattice assuming bulk

phonon scattering) used the wrong value for $\hbar\omega_{LO}^{GaAs}$ and thus considerably overestimated the scattering rate. We see from fig 4.1 that for superlattices with narrow GaAs layers the effect of phonon 'confinement' is to increase the mobility by up to a factor of two while for wider GaAs layers this effect becomes negligible. Thus phonon 'confinement' is much more important for interband scattering than for intraband scattering. The reason for this is that interband scattering involves phonons with large $q_{\parallel}$ so that scattering by interface modes is negligible and the $m = 1$ guided mode does not contribute to scattering from the first excited miniband to the lowest miniband ($2 \rightarrow 1$) as this mode has scalar potential with even symmetry. The mode which dominates $2 \rightarrow 1$ interband scattering is the m=2 guided mode (Jain and Das Sarma 1989).

4.1.2 Interface Roughness Scattering

The LO phonon limited mobility has already been determined in the previous section. However it is found that this mobility is up to an order of magnitude larger then the experimentally measured mobility (Sibille at al 1987). This suggests the prevalence of additional scattering mechanisms. In particular interface roughness (IFR) scattering has been shown to be important for parallel transport in *GaAs/AlAs* quantum wells (Sakaki et al 1987) , and we examine the role of IFR scattering on vertical transport.

The scattering rate for IFR scattering has already been derived in the previous chapter and unlike LO phonon scattering a simple formulae for the relaxation time does exist for IFR scattering. Since IFR scattering is elastic and k_z randomizing ,

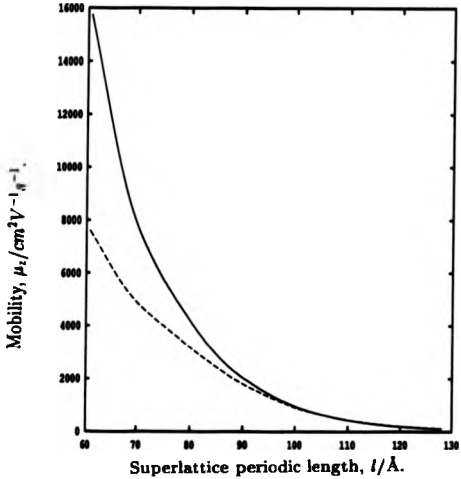

Figure 4.1: LO-phonon limited μ_z at 300 K.

Solid curve:the predicted mobility using the DCM. Broken curve: bulk phonons assumed.

i.e.

$$T(\mathbf{k}_{\parallel}, k_z \rightarrow \mathbf{k}'_{\parallel}, k'_z) = T(\mathbf{k}_{\parallel}, k_z \rightarrow \mathbf{k}'_{\parallel}, -k'_z), \tag{4.4}$$

when the electric field is applied in the growth direction the relaxation time is given by

$$\tau_r(\mathbf{k}) = \left(\frac{V}{8\pi^3}\int T(\mathbf{k},\mathbf{k}')\, d^3\mathbf{k}\right)^{-1}. \tag{4.5}$$

Note that this is only for the specific case when the electric field is applied in the growth direction. When the electric field is applied parallel to the layers the relaxation time has a significantly different form. The perturbed distribution is then given by

$$g(\mathbf{k}) = \tau_r(\mathbf{k})\frac{e}{\hbar}E_z\frac{\partial f_0}{\partial k_z}. \tag{4.6}$$

Before the mobility can be evaluated the values of the IFR parameters need to be known. Often the IFR parameters are obtained by fitting the calculations to the experimental results, however the amount of experimental data for vertical transport in *GaAs/GaAlAs* superlattices is too small to allow this. Fortunately it is possible to obtain values for the IFR parameters from other sources, it has even been possible to directly visualize the IFR (Christen et al 1988). The *GaAs/GaAlAs* interface contains terraces with steps of one monolayer height and a lateral size which is strongly dependent on growth conditions. There is good agreement on the value of the IFR height parameter Ω, this is equal to the root mean square value of the deviation of the interface from a flat plane and is found to be equal to one monolayer (Joyce et al 1986, Tanaka et al 1987, Sakaki et al 1987). The value of the IFR lateral width parameter Λ is less certain. In particular growth interruptions of a few seconds at the interfaces can significantly increase the lateral size of the plateaus (Tanaka and

Sakaki 1987, Christen et al 1988). Without growth interruptions Joyce et al (1986) deduce from RHEED measurements that the $GaAs$ grown on $GaAlAs$ surfaces have IFR with a lateral width $\Lambda_1 = 35$ Å and the $GaAlAs$ grown on $GaAs$ surface have IFR with a lateral width $\Lambda_2 = 200$ Å. Tanaka and Sakaki (1987) obtain very similar results from studies of photoluminescence data in $GaAs/GaAlAs$ quantum well. They derive values of 40 Å and 200 Å respectively for the lateral width. From measurements of mobility in a $GaAs/AlAs$ quantum well Sakaki et al (1987) derive $\Lambda_1 = 50 - 70$ Å. In fig 4.2 the results of the mobility calculations are presented using the IFR parameters deduced by Joyce at al (1986). The IFR limited mobility is very much less then the LO phonon limited mobility and thus we can conclude that in $GaAs/GaAlAs$ superlattices IFR scattering is the dominant scattering mechanism for transport in the growth direction. This is also confirmed by the temperature dependence of the measured mobility. Sibille et al (1987) found the ratio of the measured mobilities at 77 K and 300 K to be

$$\frac{\mu_z(77k)}{\mu_z(300k)} \simeq 2. \tag{4.7}$$

This result is in good agreement with calculations of the temperature dependence of the IFR limited mobility, (fig. 4.3) when Λ is taken to be 100 Å. For the LO phonon limited mobility the ratio of mobilities at 77 K and 300 K would be about 10. The agreement between experiment and theory on the magnitude of the mobility is not so good. Sibille at al (1987) measured the mobility of a 40 Å/20 Å (well width/barrier width) $GaAs/Ga_{0.7}Al0.3As$ superlattice to be about 1000 $cm^2V^{-1}s^{-1}$. Using the IFR parameters for a superlattice grown without growth interruptions (Joyce 1986) the calculated IFR limited mobility is found to be a factor of five larger, though

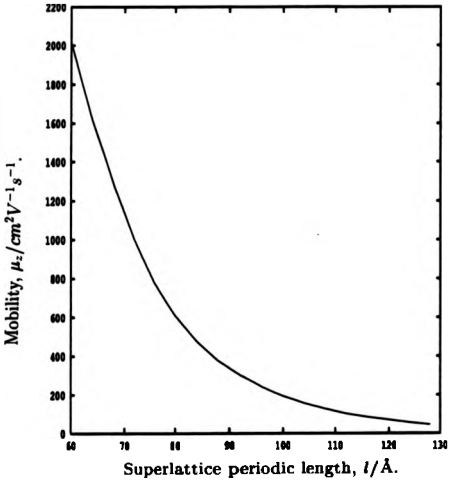

Figure 4.2: IFR limited μ_z at 300 K.

The predicted mobility using the IFR parameters of Joyce et al (1986).

the LO phonon limited mobility is a factor of twenty larger then the experimental value. However the barrier layers of the superlattice are quite narrow and the tight-binding approximation used to calculate the electron envelope functions is likely to be inadequate. Using exact envelope functions for the Kronig-Penney potential increases the scattering rate and the IFR limited mobility is then a factor of three larger than the experimental value. However in view of the uncertainty in the exact values of the IFR parameters, in particular their strong dependence on growth conditions, the agreement between experiment and theory is felt to be reasonable. The most important point is that the IFR scattering is up to an order of magnitude larger than LO phonon scattering.

In fig 4.4 the dependence of the mobility μ_s on the IFR lateral width is given. It is important to consider the effect of the IFR lateral width parameter Λ on the mobility since growth interruptions can significantly increase Λ. Tanaka and Sakaki (1987) conclude that for $x > 0.3$ only the $Ga_{1-x}Al_xAs$ grown on $GaAs$ surfaces are affected by growth interruptions , and when $x < 0.3$ both types of interfaces are affected by growth interruptions. Christen et al (1988) found that growth interruptions of 120 seconds could increase the lateral size Λ to 6-8 μm. It has been suggested that growth interruptions smooth the interface so that IFR scattering would become negligible. From fig 4.4 it is clear that growth interruptions can reduce IFR scattering. Growth interruptions of sufficiently long periods would reduce IFR scattering so that perhaps LO-phonon scattering becomes dominant.

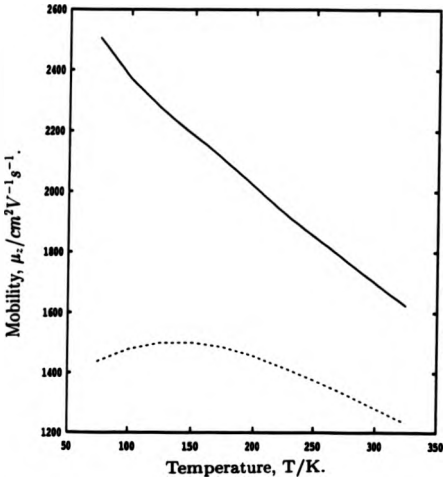

Figure 4.3: Temperature dependence of the IFR limited μ_z.

Temperature dependence of the IFR limited mobility of a superlattice with l = 60 Å and $V_0 = 250meV$. Both types of interfaces are treated as having the same IFR parameters, Ω = 3 Å and Λ = 100 Å (solid curve) or 200 Å (broken curve). Note the temperature dependence of the IFR limited $\mu_{\parallel}$ is significantly different from that shown here (e.g. see Wataya et al 1989).

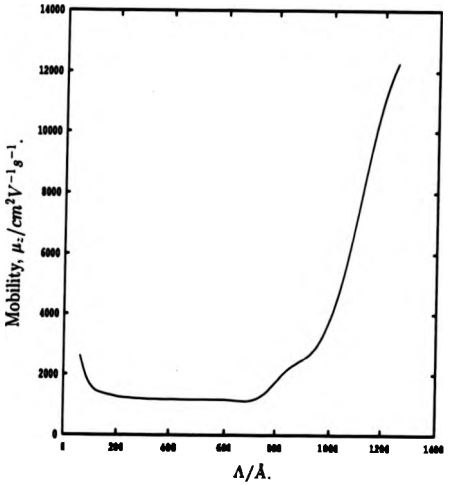

Figure 4.4: Dependence of the IFR limited μ_z on the parameter Λ. Calculated mobility at 300 K for a superlattice with $l = 60$ Å and $V_0 = 250meV$. Both types of interfaces are treated as having the same IFR parameters.

4.2 Parallel Transport

In this section we deal with the superlattice transport properties when the electric field is applied parallel to the layers. The distinct properties of the superlattice will not be as evident for parallel transport as in the case of vertical transport since the electron dispersion in the plane of the layers is taken to be free electron like with the electron having an effective mass m^* and consequently the parallel transport properties of the superlattice are similar to that in SQW and MQW structures. The mobility in these structures is generally low (Wataya et al 1989) hence very little attention has been given to their parallel transport properties. The main reason for the low measured mobilities is attributed to the poor quality of the *GaAs* grown on *GaAlAs* interface (Drummond et al 1983 , Inoue et al 1984). Much higher mobilities (at low temperatures) are found in GaAs/GaAlAs heterojunctions which contain only a single interface.

4.2.1 LO Phonon scattering

For transport in the direction parallel to the superlattice layers, the calculation of the mobility follows in the same manner as that for vertical transport. An iterative method is used to calculate the perturbed distribution function using

$$g_s(\mathbf{k}) = \tau(\mathbf{k}) \int g_s(\mathbf{k}') P(\mathbf{k}', \mathbf{k})\, d^3\mathbf{k}' + \frac{e}{\hbar} \mathbf{E}_s \frac{df_0}{d\epsilon} \frac{\hbar^2 k_s}{m^*}, \tag{4.8}$$

with $g_s(\mathbf{k})$ having a simple dependence on the angle θ in the plane of the slabs

$$g_s(\mathbf{k}) = \tilde{g}(\mathbf{k}_\parallel, \mathbf{k}_z) \cos\theta. \tag{4.9}$$

Once (4.8) has been iterated to calculate $g(\mathbf{k})$ it is a relatively simple matter to calculate the mobility. As previously determined for the case of vertical transport it is found that for superlattices with small periods l the interface modes dominates the scattering while for superlattices with wider $GaAs$ layers the guided modes dominate the scattering. Consequently we see a reduction in the LO phonon limited mobility as the superlattice period increases (fig 4.5). For comparison the mobility when the bulk phonon scattering rate (3.19) is assumed is also given. Again it is found that effect of the phonon 'confinement' is to significantly reduce the LO phonon scattering rate.

4.2.2 Interface Roughness Scattering

Sakaki et al (1987) have already shown that transport in $GaAs/AlAs$ SQWs with narrow enough wells is dominated by IFR scattering and found a characteristic L_W^6 (where L_W is the width of the $GaAs$ well) dependence in the electron mobility. For the case of vertical transport it was also found that the IFR scattering is dominant. Therefore IFR scattering may be expected to play an important role in parallel transport. Unlike the vertical transport case no simple formulae for the relaxation time approximation exists. A possible alternative is to use the iterative method (2.15). However convergence is extremely slow and more than twenty iterations are needed. Therefore we use the following equation for the relaxation time

$$\tau_r = \int P(\mathbf{k},\mathbf{k}')(1-\cos\theta)\, d^3\mathbf{k} \tag{4.10}$$

The above equation is only strictly valid when the miniband width $2\Delta \to 0$. However as we show in fig (4.6) it is in good agreement with results using the iterative method

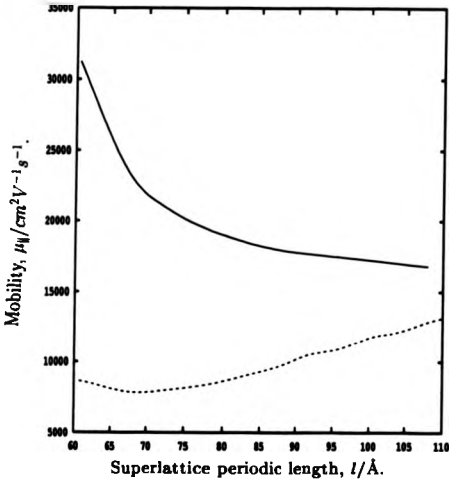

Figure 4.5: LO phonon limited $\mu_{\parallel}$ at 300 K.

Solid curve: predicted mobility using DCM. Broken curve: mobility assuming bulk phonons.

and is therefore a good approximation.

It is worth pointing out the IFR limited relaxation time is much larger for parallel transport than for vertical transport. Physically this arises because the effect of the IFR is to reflect the electrons from the interfaces consequently IFR scattering is much more important for vertical transport. For parallel transport the effect of IFR scattering is comparable to LO phonon scattering. With IFR scattering showing an approximate L_W^6 dependence and consequently more important for superlattices with narrow *GaAs* layers and LO phonon scattering more important for superlattices with wide *GaAs* layers. The combined effect of IFR and LO phonon scattering is to predict mobilities similar to those found in bulk *GaAs*, fig(4.7).

To calculate the IFR limited mobility the IFR parameters of Joyce at (1986) have been used. However it has been shown that the effect of growth interruptions can significantly affect the IFR parameters , in particular the lateral width A. In fig (4.8) the variation of the IFR limited mobility on the lateral width is given. This shows that the effect of growth interruptions are much more significant for parallel transport than for vertical transport. Tanaka and Sakaki (1987) report that for *GaAs/GaAlAs* structures with $x < 0.3$ both types of interfaces are affected by growth interruptions and thus it should be possible to reduce the effect of IFR scattering considerably so that LO phonon scattering becomes dominant. However for *GaAs/GaAlAs* structures with $x > 0.3$ the *GaAs* grown on *GaAlAs* interface is unaffected by growth interruptions and in these structures IFR would remain an important scattering mechanism, Sakaki et al (1987).

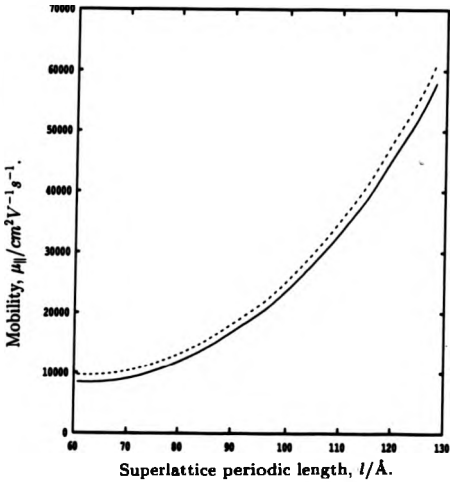

Figure 4.6: IFR limited $\mu_{\parallel}$ at 300 K.

Solid curve: predicted mobility using iterative method. Broken curve: mobility assuming relaxation time of form given by (4.10). Mobilities calculated using the IFR parameters of Joyce et al (1986).

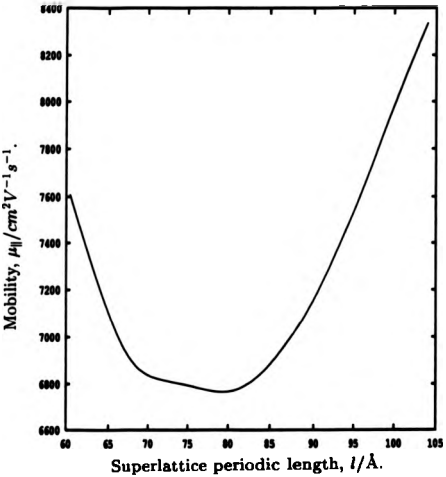

Figure 4.7: Mobility $\mu_{\parallel}$ at 300 K including both LO phonon and IFR scattering .

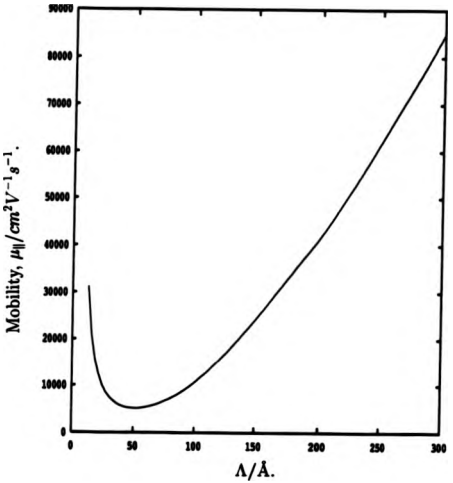

Figure 4.8: Dependence of $\mu_{\parallel}$ on IFR parameter Λ.

Mobility calculated for a superlattice with a=b, l = 60 Å and V_0 = 250meV at 300 K.

Both types of interfaces are treated as having the same IFR parameters.

Chapter 5

Calculation Of The Hall Factors

5.1 Introduction

In the preceding chapters the transport properties of a superlattice in a weak electric field have been considered. We now consider the superlattice transport properties when a weak electric field and a magnetic field are applied. There are several distinct regimes for different magnetic field strengths applied to the system. Firstly there is the low field limit, which is defined by the relationship $\omega_B\tau << 1$, where ω_B is the cyclotron frequency equal to eB/m^* and τ is a typical scattering time. The interpretation of this equation is that the electron only travels a small distance around a constant energy surface before being scattered. For this case the transport properties are most strongly influenced by the details of the scattering mechaniams. This is the regime considered in this section. Another regime is the classical high field limit where $\omega_B\tau >> 1$, but the magnetic field is not so large that quantum effects are seen in the band structure. For this situation the electrons are able to orbit constant energy surfaces many times before being scattered. Therefore

the form of these constant energy surfaces such as whether the orbits are open or closed may have the dominant influence on the transport properties (Smith et al, 1967). Perhaps the most interesting case is the quantum field limit, where Landau levels are formed, thus fundamentally altering the way the electrons behave. In low dimensional structures this leads to the observation of the quantum Hall effect (Prange and Girvin 1987).

In this chapter the superlattice transport properties in the presence of weak electric and magnetic fields are considered. In sufficiently small external fields, the effective mass theorem shows that the equations of motion are given by

$$\begin{aligned} \hbar\dot{\mathbf{k}} &= -e(\mathbf{E} + \mathbf{v} \times \mathbf{B}) \\ \mathbf{v} &= \hbar^{-1}\nabla_{\mathbf{k}}\epsilon_{\mathbf{k}}. \end{aligned} \tag{5.1}$$

The full Boltzmann equation in the steady state with magnetic field included is given by (Butcher 1973)

$$\mathbf{v}.\nabla f - \frac{1}{\hbar}[e(\mathbf{E} + \mathbf{v} \times \mathbf{B}) + \nabla\epsilon_{\mathbf{k}}].\nabla_{\mathbf{k}} f = \left(\frac{\partial f}{\partial t}\right)_{COLL} \tag{5.2}$$

and is linearized, when the temperature and Fermi level are constant throughout the superlattice, to give

$$-\frac{e}{\hbar}\mathbf{E}.\nabla_{\mathbf{k}} f_0 - (\mathbf{v} \times \mathbf{B}).\nabla_{\mathbf{k}} g = \left(\frac{\partial g}{\partial t}\right)_{COLL}. \tag{5.3}$$

In the absence of a thermal gradient, the electric current when external electric and magnetic fields are applied to a cubic crystal (Butcher, 1973)

$$\mathbf{J} = \sigma_0\mathbf{E} + \alpha\mathbf{E} \times \mathbf{B} + \beta B^2\mathbf{E} + \gamma(\mathbf{B}.\mathbf{E}).\mathbf{B} + \delta D\mathbf{E} \tag{5.4}$$

where D is a diagonal tensor with $D_{ii} = B_i^2$. The coefficients in the expression above are not measured directly, rather the coefficients in the corresponding expression for

E are measured.

$$\mathbf{E} = \rho_0 \mathbf{J} - R\mathbf{J} \times \mathbf{B} + \rho_0[b\mathbf{B}^2\mathbf{J} + c(\mathbf{B}.\mathbf{J})\mathbf{B} + d\mathbf{D}.\mathbf{J}] \tag{5.5}$$

where ρ_0 is the low field resistivity in zero magnetic field, R is the Hall constant and b, c, d are called the Seitz magnetoresistance coefficients.In this chapter we deal with the calculation of the Hall constant.

To solve the Boltzmann equation with a magnetic field present, it is often written in terms of operators (Smith et al 1967). The linearized Boltzmann equation can be written in the form

$$(C + \Omega')\phi = -e\mathbf{E}.\mathbf{v}\frac{df_o}{d\epsilon}. \tag{5.6}$$

The function $\phi(\mathbf{k}, r)$ can be related to $g(\mathbf{k}, r)$ the first order perturbation to the distribution function by

$$\phi(\mathbf{k}) = -g(\mathbf{k})\left(\frac{df_o}{d\epsilon}\right)^{-1}. \tag{5.7}$$

The operators C and Ω' are the collision and magnetic operators respectively, defined by

$$C\phi = \left(\frac{\partial g}{\partial t}\right)_{COLL} \tag{5.8}$$

$$\Omega'\phi = -\frac{df_0}{d\epsilon}\frac{e}{\hbar}(\mathbf{v} \times \mathbf{B}).\nabla_k\phi$$

The formal solution for ϕ is then given by

$$\phi = -(C + \Omega')^{-1}e\mathbf{E}.\mathbf{v}\frac{df_0}{d\epsilon}. \tag{5.9}$$

The most common approach to solve the Boltzmann transport equation with a magnetic filed present is to use the Jones-Zener expansion (Smith et al 1967). This method is applicable when the relaxation time is known. In the relaxation time

approximation the collision operator is given by

$$C = \frac{df_0}{d\epsilon_k}\tau_r^{-1} \tag{5.10}$$

and the formal solution of the linearized Boltzmann transport equation is found to be

$$\phi = -[1 - \tau_r\Omega + (\tau_r\Omega)^2 - ...]\tau_r e\mathbf{E}.\mathbf{v} \tag{5.11}$$

where

$$\Omega = \frac{e}{\hbar}(\mathbf{v} \times \mathbf{B}).\nabla_k. \tag{5.12}$$

The operator equation (5.11) is similar to the geometric series

$$(1 + x)^{-1} = 1 - x + x^2 - ... \tag{5.13}$$

which is known to converge only when $|x| < 1$. Similarly there is a limit on the convergence of (5.11). The magnitude of $(\tau_r\Omega)$ increases linearly with magnetic field, consequently to obtain convergence of (5.11) an upper limit is imposed on the magnetic field strength. In practice this limit is very difficult to determine however we shall assume that the magnetic field is below this limit and that the term low magnetic field region is understood to comply with this requirement as well as the condition, $\omega_B\tau << 1$.

To solve the Jones-Zener expansion it is then necessary to find the form of the relaxation time. However in the previous chapters we have calculated the first order perturbation to the distribution function $g(\mathbf{k})$ and not the relaxation time. Warren (1988) has developed a formalism similar to the Jones-Zener expansion, but which only requires the functions $g(\mathbf{k})$ to be known for three mutually perpendicular directions of the electric field (with no magnetic field present) to calculate the Hall

constants for the system. Since we have already solved the zero magnetic field Boltzmann transport equation it is a relatively simple matter to calculate the Hall constants.

5.2 Method Of Calculation

The formalism to calculate the Hall factors has already been developed by Warren(1988). Here we correct some errors in the original formulae and describe the method for calculating the Hall Factors in a superlattice. This is a novel method that can be used for many different systems and is particularly useful when the Jones-Zener expansion cannot be used. Using this method little further work is necessary if the zero magnetic field Boltzmann equation has already been solved.

The superlattice system has cylindrical symmetry, Consequently the macroscopic current density $\mathbf{J}$ and the electric field $\mathbf{E}$ take the form

$$\begin{aligned} \mathbf{J} &= \mathbf{J}_{\parallel} + \mathbf{J}_{z} \\ &= \sigma_{\parallel}\mathbf{E}_{\parallel} + \sigma_{z}\mathbf{E}_{z} + \zeta\mathbf{E}\times\mathbf{B}_{\parallel} + \eta\mathbf{E}\times\mathbf{B}_{z} \end{aligned} \tag{5.14}$$

where $\mathbf{J}_{\parallel} = (J_x, J_y, 0)$, $\mathbf{J}_{z} = (0, 0, J_z)$ and $\mathbf{E}_{\parallel}, \mathbf{E}_{z}$ and $\mathbf{B}_{\parallel}, \mathbf{B}_{z}$ have a similar interpretation. The transport coefficients $\sigma_{\parallel}, \sigma_{z}, \zeta, \eta$ in (5.14) are expressed in terms of appropriate solutions of Boltzmann's equation in section 3. The associated Hall factors may be obtained by solving (5.14) to express $\mathbf{E}$ in terms of $\mathbf{J}$ when $\mathbf{B}$ is small. We find that

$$\begin{aligned} \mathbf{E}_{\parallel} &= \sigma_{\parallel}^{-1}\left[\mathbf{J}_{\parallel} - \zeta\sigma_{z}^{-1}\mathbf{J}_{z}\times\mathbf{B}_{z} - \eta\sigma_{\parallel}^{-1}\mathbf{J}_{\parallel}\times\mathbf{B}_{z}\right] \\ \mathbf{E}_{z} &= \sigma_{z}^{-1}\left[\mathbf{J}_{z} - \zeta\sigma_{\parallel}^{-1}\mathbf{J}_{\parallel}\times\mathbf{B}_{\parallel}\right]. \end{aligned} \tag{5.15}$$

The two independent Hall constants involved in these equations are

$$\begin{aligned} R^{xyz} &= \frac{E_x}{J_y B_z} = -\eta \sigma_\parallel^{-2} \\ R^{xxz} &= \frac{E_x}{J_x B_z} = -\zeta \sigma_\parallel^{-1} \sigma_x^{-1} \\ R^{xxz} &= \frac{E_y}{J_x B_z} = -\zeta \sigma_\parallel^{-1} \sigma_x^{-1}. \end{aligned} \tag{5.16}$$

The Hall factors are simply related to the Hall constants by

$$r^{ijk} = -neR^{ijk} \tag{5.17}$$

where the first superscript i gives the direction of the Hall field $\mathbf{E}^H$ the second superscript the direction of the current density J and the third superscript k gives the direction of the magnetic field B. To calculate ζ and η we begin with the formal solution to the Boltzmann transport equation

$$\phi = -(C + \Omega')^{-1} e\mathbf{E}.\mathbf{v} f_0'. \tag{5.18}$$

Now if we start with the case of no magnetic field present, we can write the solution in terms of the inverse collision operator $G_0 \equiv C^{-1}$.

$$\phi_0 = -G_0 e\mathbf{E}.\mathbf{v} f_0'. \tag{5.19}$$

It is worth noting here that the solution in an electric field $\mathbf{E}'$ is similarly given by

$$\phi_0' = -G_0 e\mathbf{E}'.\mathbf{v} f_0'. \tag{5.20}$$

For the case where a magnetic field is present, the solution is given by

$$\phi = -Ge\mathbf{E}.\mathbf{v} f_0' \tag{5.21}$$

where the operator $G \equiv (C + \Omega')^{-1}$. Performing a small amount of manipulation (Warren 1988), we find

$$\begin{aligned} G &= (1 + G_0\Omega')^{-1} G_0 \\ &\cong (1 - G_0\Omega') G_0 \end{aligned} \tag{5.22}$$

to first order in $\mathbf{B}$. Then the solution ϕ is given by

$$\phi = -(G_0 - G_0\Omega' G_0)e\mathbf{E}.\mathbf{v}f_0'. \tag{5.23}$$

The term in ϕ of interest is the one that is linear in the magnetic field and which dominates the resultant Hall current.

$$\begin{aligned} \Delta\phi \equiv \phi - \phi_0 &= -G_0\Omega' G_0 e\mathbf{E}.\mathbf{v}f_0' \\ &= -G_0\Omega'\phi_0. \end{aligned} \tag{5.24}$$

The resultant Hall current is given by

$$\mathbf{J}^H = (e/4\pi^3)\int d\mathbf{k}\ \mathbf{v}f_0' G_0\Omega'\phi_0. \tag{5.25}$$

To gain insight into this result,we take its scalar product with another force field $e\mathbf{E}'$ where $\mathbf{E}'$ remains arbitrary for the moment. Thus we obtain

$$e\mathbf{E}'.\mathbf{J}^H = (e/4\pi^3)\int d\mathbf{k}\ (e\mathbf{E}'.\mathbf{v}f_0')G_0(\Omega'\phi_0). \tag{5.26}$$

Since G_0 is a symmetric operator, the function on the left of G_0 in (5.26) may be interchanged with G_0 to give

$$e\mathbf{E}'.\mathbf{J}^H = -(e/4\pi^3)\int d\mathbf{k}\ \phi_0'\Omega'\phi_0. \tag{5.27}$$

We may use this result to obtain ζ and η in (5.14). Thus setting $\mathbf{B} = (B_z, 0, 0)$ and $\mathbf{E} = (0, 0, E_z), \mathbf{E}' = (0, E_y', 0)$ gives

$$\zeta = -(1/4\pi^3)\int d\mathbf{k}\ \left(\frac{\phi_y'}{E_y'}\right)\frac{\Omega_z'}{B_z}\left(\frac{\phi_z}{E_z}\right) \tag{5.28}$$

where ϕ_z, Ω_z' and ϕ_y' denote ϕ_0, Ω' and ϕ_0' for the above values of $\mathbf{E}, \mathbf{B}$ and $\mathbf{E}'$ respectively. Similarly, we find that

$$\eta = -(1/4\pi^3)\int d\mathbf{k}\ \left(\frac{\phi_z'}{E_z'}\right)\frac{\Omega_z'}{B_z}\left(\frac{\phi_y}{E_y}\right). \tag{5.29}$$

Once ϕ_x, ϕ_y and ϕ_z have been determined by iterative numerical solution of the appropriate linearized Boltzmann equations with $\mathbf{B} = 0$, we may use (5.28,5.29) to calculate ζ and η. These results, together with the mobility calculations allow us to evaluate the Hall factors.

5.3 Results

In this section we present results for the calculation of the Hall factors. Unlike the calculations of Warren (1988) we use the correct scattering rates (3.47,3.48) including the effect of optical phonon 'confinement' and also scattering by interface roughness. As might be expected from the cylindrical symmetry of the problem we find two independent Hall factors, both of which remain close to one. Numerical results are presented in fig 5.1, for a temperature T=300 K and assuming non-degenerate statistics, both optical phonon and IFR scattering are included. When the magnetic field is applied perpendicular to the interface planes, the Hall factor r^{xy} remains of the order of one with some minor structure when the superlattice period $l = 80$ and 90 Å. When the magnetic field is applied parallel to the interface planes, the Hall factor r^{zz} is again close to one, but exhibits a peak near $l = 80$ Å. A simple kinetic theory would predict both Hall factors equal to one and it is difficult to interpret the exact reason for the deviation of the Hall factors from one. Both the non-parabolicity of the energy band structure and the wavevector dependence of the relaxation time contribute to the deviation of the Hall factors from one. For a system with with spherically symmetric energy bands and a relaxation time that

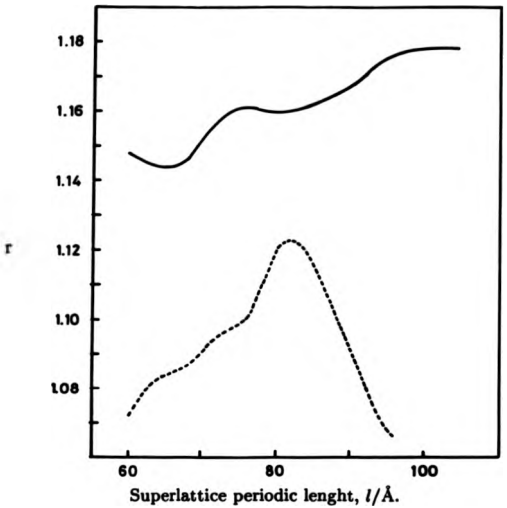

Figure 5.1: Calculated Hall factors at 300 K.

Hall factors calculated including both IFR scattering and LO phonon scattering. Solid curve: magnetic field applied in the growth direction, Hall factor r^{zyx}. Broken curve: magnetic field applied parallel to the interface layers, Hall factor $r^{xxy} = r^{yxx}$.

is only dependent on energy $\tau_r = \tau_r(\epsilon_k)$, the Hall factor is given by

$$r = \frac{<\tau^2>}{<\tau>^2} \tag{5.30}$$

where the averaging bracket is defined as

$$<g(\epsilon_k)> = \frac{\int_0^\infty \epsilon_k^{3/2} g(\epsilon_k) \frac{df_0}{d\epsilon_k} d\epsilon_k}{\int_0^\infty \epsilon_k^{3/2} \frac{df_0}{d\epsilon_k} d\epsilon_k}. \tag{5.31}$$

This is a standard result that can be readily derived from the present theory (Warren 1988). Thus the deviation of the Hall factor from one depends on the energy dependence of the relaxation time and the actual value of the Hall factors depends on the predominance of the various scattering mechanisms.

Chapter 6

Conclusions and Suggestions

The objective of this work has been to improve the understanding of electron transport in $GaAs/GaAlAs$ superlattices and to examine the validity of the Boltzmann transport formalism used to describe it. In this chapter the final conclusions are presented and suggestions made for future work.

6.1 Conclusions

It is clear from the introductory chapters that the physics of superlattices displays many interesting features. In particular the prospect of observing Bloch oscillations and negative differential resistance with implications for device applications have produced much interest in these structures. We have shown that there is considerable experimental evidence that electron transport in superlattices in the growth direction can proceed by extended Bloch states. Consequently the Boltzmann transport formalism has been used to calculate the electron mobilities. The main challenge in calculating the mobilities has been to identify the important electron scattering

mechanisms and to determine the form of the scattering rates. Once this is done the the calculation of the mobility is straight forward. Though care must be taken as often no simple formulae for the relaxation time exists. In this case we have shown how an iterative method may be used. The assumption that the relaxation time is equal to the electron lifetime can lead to large errors, for longitudinal-optical phonon scattering this assumption can underestimate the mobility by about a factor of two. For interface roughness scattering the mobility parallel to the superlattice layers is underestimated by an order of magnitude by this approximation.

The dominant scattering mechanism in bulk *GaAs* at room temperature is LO-phonon scattering. Therefore it has been expected to be an important scattering mechanism in a *GaAs/GaAlAs* superlattice. The original calculations of the LO phonon scattering assumed that the optical phonons were unperturbed by the superlattice structure and used the bulk LO phonon scattering rate. However this assumption is incorrect and we have shown that there is a large amount of experimental and calculated data that shows that the optical phonon modes are strongly perturbed by the superlattice structure, leading to a strong modification of the electron-LO phonon scattering rate. For the purposes of transport calculations, simple continuum models are used to describe the superlattice phonon modes. However no unambiguous formulation of the boundary conditions exists for these continuum models. The most commonly used boundary conditions are either the standard electrostatic boundary conditions which are used by the dielectric continuum model (DCM) or the hydrodynamic boundary conditions used by the hydrodynamic continuum model. There has been considerable controversy as to which, if either, of these two models can give a correct description of electron-LO phonon scattering in

a superlattice. Comparing the results of the continuum models with realistic microscopic models shows that neither of the continuum models gives a good description of the optical displacement of the ions. However the work of Huang and Zhu (1988) shows that the DCM does give a good description of the scalar potential associated with the optical displacement and can therefore give a correct description of the electron-LO phonon scattering rate in a superlattice. Calculations of electron energy relaxation times in a quantum well using the DCM are also in good agreement with experiment and it has been shown that the 'confinement' of the optical phonon modes leads to a reduction of up to an order of magnitude of the electron energy relaxation time (Jain and Das Sarma 1989). The intraband scattering rate is not so strongly affected by the 'confinement' of the optical phonon modes, and the scattering is reduced by a factor of two for both transport parallel and perpendicular to the superlattice layers. As might be expected this reduction is more important for superlattices with narrow layers and becomes insignificant for superlattices with wide layers.

Comparing the calculated LO phonon limited electron mobility in the growth direction with experimental data, we find that the predicted mobility is larger by a factor of twenty. The experimentally measured mobility is too large to be due to hopping transport consequently this suggests the prevalence of other scattering mechanisms. We have shown that the unavoidable roughness of the superlattice interfaces can account for this additional scattering. Interface roughness (IFR) scattering is particularly interesting since it is not found in bulk materials and the IFR scattering is much more important for transport in the growth direction than for transport parallel to the interface planes. The reason for this is that the effect of

the IFR is to reflect the electrons from the interfaces. IFR scattering is found to be the dominant scattering mechanism in limiting the mobility in the growth direction. Unfortunately a detailed comparison of the magnitude of the calculated mobilities with the experimental values is difficult due to uncertainties in the IFR parameters. There are two IFR parameters, one to describe the root mean square height of the deviation of the interface from a flat plane Ω and the other Λ to describe the lateral size of the IFR and these parameters have a strong influence on the actual magnitude of the mobility. This matter is further complicated by the effect of growth interruptions at the interfaces during the growth of the superlattice. These growth interruptions have a significant effect on the IFR parameter Λ. The effect of growth interruptions is to reduce the IFR scattering and for sufficiently long growth interruption times this effect can result in LO-phonon scattering becoming dominant in a $GaAs/Ga_{0.7}Al_{0.3}As$ superlattice. However, in a $GaAs/AlAs$ superlattice IFR scattering would remain important since the $GaAs$ grown on $Ga_{1-x}Al_xAs$ interface is unaffected by growth interruptions provided $x > 0.3$ (Tanaka and Sakaki 1987).

For transport parallel to the interfaces the effect of IFR scattering is not as important as for transport in the growth direction. For a superlattice grown without growth interruptions the IFR scattering is of about the same importance as LO phonon scattering. With IFR scattering being the most important for superlattices with narrow $GaAs$ layers and LO phonon scattering more important for wide $GaAs$ layers. Consequently the effect of this is an electron mobility in a $GaAs/Ga_{0.7}Al_{0.3}As$ superlattice, similar to that found in bulk $GaAs$. Again the effect of growth interruptions is to reduce the IFR scattering so that LO phonon scattering becomes the dominant scattering mechanism for transport parallel to the layers. We have also

calculated the Hall factors. We find two independent Hall factors both of which remain close to one.

6.2 Prospects for further developments

We have tried to develop a simple formalism to calculate the low field transport properties of a non degenerate electron gas in a *GaAs/GaAlAs* superlattice. The present work can be extended by relaxing some of the approximations we have made. In particular the Kronig-Penney model can be solved exactly to calculate the electron envelope function rather than using a tight binding formalism, additionally the difference in effective mass between the *GaAs* and *GaAlAs* layers can also be included in the calculations. This can be important for IFR scattering rate since this depends on the value of the envelope function at the interfaces. An alloy material such as bulk *GaAlAs* has two LO modes and two TO modes and it would also be desirable to include this feature of *GaAlAs* into future work. We can also consider the transport properties as the electron concentration is increased. An effect of this would be the need to include screening and interband scattering.

Perhaps the most interesting approach would be to calculate the hot electron transport properties of the superlattice. In this regime we can expect to see negative differential resistivity(NDR). NDR has already been observed in a superlattice and it is claimed that this is due to the effect originally proposed by Esaki and Tsu (Sibille et al 1990). Unfortunately there is little hope for useful analytical calculations in this regime. The most physically transparent numerical approach is the Monte carlo simulation. Very high electric fields applied in the growth direction can also induce

localisation of the electron states. A study which incorporates transport both by extended states and localised states and can describe the change from Bloch to hopping transport represents a considerable challenge.

Appendix A

Kronig-Penney Model

Using the tight-binding theory in the nearest neighbor approximation the electron envelope wavefunction is written as

$$F(\mathbf{r}) = \left(\frac{l}{V}\right)^{1/2} \exp(i\mathbf{k}_{\parallel}.\mathbf{x}_{\parallel}) \sum_{n} \phi(z - nl) \exp(ik_z nl) \tag{A.1}$$

where $\phi(z)$ is the eigenfunction for the Hamiltonian of a single potential well of width $2a$ and height V_0. The form of $\phi(z)$ is given by;

$$\phi(z) = \begin{cases} C\exp(\lambda z) & z < -a \\ A\cos(k_0 z) & -a < z < -a \\ C\exp(-\lambda z) & z > a \end{cases} . \tag{A.2}$$

Where $\lambda^2 = (V_0 - \epsilon_0)2m^*/\hbar^2$ and $\epsilon_0 = \hbar^2 k_0^2/2m^*$. Note that when $z \geq a$

$$\phi(z) = -\frac{1}{\lambda}\frac{d\phi}{dz}, \tag{A.3}$$

this expression has been used when calculating the interface roughness scattering rate. The values for the parameters in the equation for $\phi(z)$ are obtained by applying standard boundary conditions. By matching $\phi(z)$ at $z = a$ we obtain

$$C = A\cos(k_0 a)\exp(\lambda a) \tag{A.4}$$

and A is found by normalizing $\phi(z)$. By matching the derivative $d\phi/dz$ at $z = a$ and $z = -a$ we find

$$\tan(k_0 a) = \frac{\left(\frac{2m^* V_0 a^2}{\hbar^2} - k_0^2 a^2\right)^{1/2}}{k_0 a}. \tag{A.5}$$

The above equation is solved numerically, but in the tight-binding limit it is approximately given by

$$k_0 a \simeq \frac{\pi}{2} \frac{\beta}{\beta + 1} \tag{A.6}$$

where $\beta = (2m^* V_0 a^2 \hbar^{-2})^{1/2}$. similarly

$$A^2 \simeq \frac{1}{a} \frac{\beta}{\beta + 1}. \tag{A.7}$$

In the nearest neighbor approximation the miniband structure of the superlattice can be written as

$$\epsilon_k = \frac{\hbar^2 k_\parallel^2}{2m^*} + \Delta(1 - \cos k_z l). \tag{A.8}$$

2Δ is the miniband width and is calculated from the superlattice dispersion relation (1.7). However an approximate analytic form for delta can be obtained from the tight-binding approximation (Kittel 1953)

$$\Delta = 2 \int \phi(z) H_{KP} \phi(z - l)\, dz \tag{A.9}$$

where H_{KP} is the Hamiltonian for the Kronig-Penney potential. Solving the above integral we find

$$\Delta \simeq 4A^2 b \frac{k_0^2}{\lambda^2} \sin^2(k_0 a) \epsilon_0 \exp(-2\lambda b). \tag{A.10}$$

The important point to note about the above equation is that the dependence of Δ on the width of the superlattice layers will be dominated by the $\exp(-2\lambda b)$ term. This explains the form of the miniband width given in fig. 1.2 .

We can investigate the effect of this highly anisotropic miniband structure on the superlattice transport properties using a simple model, a relaxation time which is independent of energy or wavevector is assumed. Then for transport parallel to the superlattice layers the mobility is given by

$$\mu_{\parallel} = \frac{\tau e}{m^*}. \tag{A.11}$$

For transport in the growth direction the effect of the miniband structure is more obvious. Using the Boltzmann transport equation the mobility is given by

$$\mu_z = -\frac{e\tau\Delta^2 l^2}{\hbar^2} \frac{\int_0^\infty \frac{\partial f_0}{\partial \epsilon} d\epsilon \int_{-\alpha}^{+\alpha} \sin^2(k_z l)\, dk_z}{\int_0^\infty f_0\, d\epsilon \int_{-\alpha}^{+\alpha} dk_z} \tag{A.12}$$

where

$$\alpha = \frac{1}{l}\cos^{-1}\left(1 - \frac{\epsilon}{\Delta}\right) \quad \epsilon < 2\Delta$$

$$\alpha = \frac{\pi}{l} \qquad \epsilon > 2\Delta \tag{A.13}$$

The above equation for μ_z has a simple form when $\Delta >> k_B T$. Then the superlattice miniband structure can be written as

$$\epsilon_k = \frac{\hbar^2 k_\parallel^2}{2m^*} + \frac{\hbar^2 k_z^2}{2m_z^*} \tag{A.14}$$

where $m_z^* = \hbar^2/(\Delta l^2)$ and for this case the approximation $\alpha = (2m_z^* \epsilon_k \hbar^{-2})^{1/2}$ is used. Then the mobility is given by

$$\mu_z = e\tau \frac{\Delta l^2}{\hbar^2}. \tag{A.15}$$

The mobility also has a simple form when $\Delta << k_B T$. In this case we use the approximation $\alpha = \pi/l$. The form of the mobility is then found to be

$$\mu_z = e\tau \frac{\Delta l^2}{\hbar^2} \frac{\Delta}{2k_B T}. \tag{A.16}$$

This is a particularly interesting result since the mobility shows a temperature dependence. Usually the temperature dependence of the mobility is due to the form of the scattering mechanisms. However in this case the temperature dependence is due to the form of the miniband structure. This 'thermal saturation' of the band transport has been observed experimentally by Brozak et al 1990.

Appendix B

Modified Dielectric Continuum Model

We have shown in chapter 3 that the dielectric continuum model (DCM) gives a good description of the scalar potential associated with the LO modes of the superlattice but a poor description of the displacement of the ions. In this section a modified DCM is introduced which is shown to give a good description of both the displacement of the ions and the scalar potential. The longitudinal optical vibrations have associated with them an electric field and a scalar potential. Maxwell's equations when we neglect retardation effects are given by

$$\nabla.\mathbf{D} = 0 \ , \ \nabla \times \mathbf{E} = 0 \qquad \text{(B.1)}$$

and we obtain the following condition on the scalar potential

$$\kappa_i(\omega)\nabla^2\nu(\mathbf{r}) = 0. \qquad \text{(B.2)}$$

Where $\kappa_i(\omega)$ is the dielectric function in material i. We apply this model to a $GaAs/AlAs$ single quantum well of width $2a$ centered at $z = 0$. From the periodicity

of the system Bloch's condition implies that the scalar potential associated with the LO modes can be written as

$$\nu(\mathbf{r}) = \exp(i\mathbf{q}_{\parallel}.\mathbf{x}_{\parallel})\Phi(z). \tag{B.3}$$

Thus (B.2) is satisfied when

$$\Phi(z) = [A_G \exp(iqz) + B_G \exp(-iqz)]\delta_{\epsilon_s(\omega),0} + A_I \exp(q_{\parallel}z) + B_I \exp(-q_{\parallel}z). \tag{B.4}$$

We have written $\Phi(z)$ in an unusual form, previous calculations of the dielectric continuum model have taken either the first or second term on the right hand side of (B.4) but have not allowed mixing of the two terms. In the absence of mixing standard Fuchs and Kliewer like modes are obtained. However we show below that when mixing is allowed it is possible to obtain results in good agreement with realistic microscopic models. Since we now have four unknown coefficients in $\Phi(z)$ there is a need for additional boundary conditions as well as the usual electrostatic boundary conditions.It has been shown that for systems where the bulk LO phonon branches of the constituent materials do not overlap (eg $GaAs/AlAs$) it sufficient to demand that u_z and $u_{\parallel}$ both have nodes at the interfaces (Tsuchiya et al 1989). The optical displacement vector is derived from the scalar potential using the Born and Huang phenomenological equations.

$$\mathbf{u}_{LO}(\mathbf{r},\omega) = c_t \nabla \nu(\mathbf{r}). \tag{B.5}$$

Where c_t can be derived from the Born and Huang equations and is material dependent.

Using the above equations it is a simple matter to derive the form of the scalar

potential. When $\omega = \omega_{LO}^{GaAs}$,

$$\Phi(z) = \begin{cases} A_f^{AlAs}\exp(q_\parallel z) & AlAs \quad z < -a \\ A_f^{GaAs}\exp(q_\parallel z) + B_f^{GaAs}\exp(-q_\parallel z) & \\ \quad + A_G\exp(iqz) + B_G\exp(-iqz) & GaAs \quad -a < z < a \\ B_f^{AlAs}\exp(-q_\parallel z) & AlAs \quad z > a \end{cases} \tag{B.6}$$

The coefficients in the above equation are obtained by applying the boundary conditions. From the electrostatic boundary condition that D_z (Maxwell's displacement vector in the z direction) is continuous at an interface we obtain that $A_f^{AlAs} = B_f^{AlAs} = 0$ (note this is only true when $\omega = \omega_{LO}^{GaAs}$). When this is the case the remaining boundary conditions are then satisfied when $\Phi(z)$ and $\partial\Phi/\partial z$ have nodes at the interfaces. We find that all the modes have a scalar potential which is either symmetric or anti-symmetric in the growth direction. For the symmetric(anti-symmetric) modes we have $A_f^{GaAs} = B_f^{GaAs}$ ($A_f^{GaAs} = -B_f^{GaAs}$), $A_G = B_G$ ($A_G = -B_G$). Thus for the symmetric modes

$$\begin{aligned} A_f^{GaAs}\cosh(q_\parallel a) + A_G\cos(qa) &= 0 \\ q_\parallel A_f^{GaAs}\sinh(q_\parallel a) - A_G q\sin(qa) &= 0. \end{aligned} \tag{B.7}$$

To simplify the notation we define $q_s \equiv q$,$A_s \equiv 2A_G$ and $C_s \equiv 2A_f^{GaAs}$.We then find that $q_s\tan(q_s a) = -q_\parallel\tanh(q_\parallel a)$ and $C_s\cosh(q_\parallel a) = -A_s\cos(q_s a)$. In the long wavelength limit ($q_\parallel \to 0$) this reduces to $q_s \to m\pi/a$ and $C_s \to -A_s(-1)^m$.

For the anti-symmetric modes

$$\begin{aligned} A_f^{GaAs}\sinh(q_\parallel a) + iA_G\sin(qa) &= 0 \\ q_\parallel A_f^{GaAs}\cosh(q_\parallel a) + iqA_G\cos(qa) &= 0. \end{aligned} \tag{B.8}$$

Again to simplify the notation we define $q_a \equiv q$, $A_a \equiv 2iA_G$ and $C_a \equiv 2A_f^{GaAs}$. We find that $q_a\cot(q_a a) = q_\parallel\coth(q_\parallel a)$ and $C_a\sinh(q_\parallel a) = -A_a\sin(q_a a)$. In the long

wavelength limit this reduces to $\tan(q_n a) = q_n a$ and $C_n q_\parallel a = -A_n \sin(q_n a)$. The exact values of q_n and C_n are obtained numerically and we find that in the long wavelength limit $q_n a \simeq n\pi/2$ where n=3,5,7 ... and $C_n q_\parallel a \simeq -A_n(-1)^{\frac{n-1}{2}}$.

Thus we can write for symmetric modes, when $\omega = \omega_{LO}^{GaAs}$,

$$\Phi(z) = \begin{cases} A_n \cos(q_n z) + C_n \cosh(q_\parallel z) & -a < z < a \\ 0 & otherwise \end{cases} \qquad \text{(B.9)}$$

For anti-symmetric modes

$$\Phi(z) = \begin{cases} A_n \sin(q_n z) + C_n \sinh(q_\parallel z) & -a < z < a \\ 0 & otherwise \end{cases} \qquad \text{(B.10)}$$

These new modes are the analogue of the Fuchs and Kliewer guided modes. In fact similar expressions for the analytical form of $\Phi(z)$ (B.9,B.10) have already been guessed by Huang and Zhu(1988). They assumed that $\Phi(z)$ could be written for the symmetric (anti-symmetric) modes as a cosine (sine) term plus a constant (linear in z) term and applied the boundary conditions that $\Phi(z)$ and $\partial\Phi/\partial z$ disappear at the interfaces. Their simple analytical expressions for $\Phi(z)$ were found to fit well the results of their microscopic model in the long wavelength limit ($q_\parallel \to 0$). However our model is more general and can be extended to the case when the scalar potential does not disappear at the interfaces such as the case of interface modes or systems where the bulk LO phonon branches of the constituent materials overlap (eg InAs/GaSb). Our model is shown to follow simply from the DCM and explicitly satisfies (B.2) whereas the simple analytical expressions of Huang and Zhu (1988) have been guessed.

This is not the first study to consider the mixing of guided and interface modes. Chu and Chang (1988) have already suggested this, however they assumed that mix-

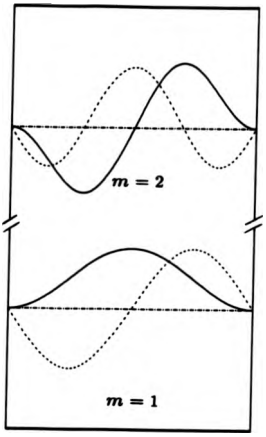

Figure B.1: Results of modified DCM.

Solid curve: W_1. Broken curve: W_2.

ing could only occur when spatial dispersion of the phonon modes was included and they were unsure what the additional boundary conditions should be, consequently no calculations were performed. Our model does not include spatial dispersion (since the Born and Huang equations do not include spatial dispersion) but we have shown that mixing can still occur when $\omega = \omega_{LO}^{GaAs}$. If we include spatial dispersion, mixing will also occur at other frequencies and this is likely to strongly affect the Fuchs and Kliewer like interface modes. It is known that the dielectric continuum model gives a very good description of the frequencies of the interface modes and the scalar potential associated with them however the actual form of the optical displacement vector is very poorly described, compared to realistic microscopic models. We may speculate that when mixing is allowed agreement with realistic microscopic models will improve significantly. However actual calculations are beyond the scope of this thesis.

Reference

Ando T. (1977) *J. Phys. Soc. Jpn.* **43** 1616

Ando T. (1982) *J. Phys. Soc. Jpn.* **51** 3900

Ando T., Fowler A.B. and Stern F. (1982) *Rev. Mod. Phys.* **54** 437

Babiker M. (1986) *J. Phys. C* **19** 683

Baroni S., de Gironcoli S., Giannozz P., (1990) *Phys. Rev. Lett.* **65** 84

Bastard G. (1981) *Phys. Rev. B* **24** 10 5693

Bastard G. (1982) *Phys. Rev. B* **25** 7584

Bishop D.J., Tsui D.C. and Dynes R.C. (1985) in *Localization, Interaction, and Transport Phenomena* (Eds. Kramer B., Bergmann G. and Bruynseraede) (Berlin: Springer)

Born M. and Huang K. (1962) *Dynamical Theory of Crystal Lattices* (Oxford : OUP)

Brozak G., Helm M., DeRosa F., Perry C.H., Kosa M., Bhat R. and Allen S.J. *Phys. Rev. Lett.* **64** 3163

Bruesch P. (1982) *Phonons: Theory and Experiment vol. 1* (Berlin : Springer)

Butcher P.N. (1973) *Electrons in Crystalline Solids* (Vienna : IAEA)

Butcher P.N. (1986) in *Crystalline Semiconducting Materials and Devices* (Eds. Butcher P.N., March N.H. and Tosi M.P.) (Plenum)

Bylander D.M. and Kleinman L. (1987) *Phys. Rev. Lett.* **59** 2091

Calecki D., Palmier J.F. and Chomette A. (1984) *J. Phys. C* **17** 5017

Capasso F., Khalid M. and Cho A.Y. (1986) *J. Quantum Elect.* **QE-22** 1853

Capasso F. (1987) in *Multiquantum Wells, Selective Doping and Superlattices. Semiconductors and Semimetals* **24** (Ed. Dingle R.)

Cardona M. (1989) *Superlatt. Microstruct.* **5** 27

Chang L.L., Esaki L., Howard W.E. and Ludeke R. (1973) *J. Vac. Sci. Technol.* **10** 11

Christen J., Bimberg D., Fukunaga T., Nakashima H., Mars D.E. and Miller J.N. (1988) in *Physics and Technology of Submicron Structures* (Eds. Heinrich H., Bauer G. and Kuchar F.) (Berlin : Springer)

Chu H. and Chang Y. (1988) *Phys. Rev. B* **38** 12 369

Deveaud B., Shah J., Damen T.C., Lambert B. and Regreny A. (1987) *Phys. Rev. Lett.* **58** 2582

Dingle R., Weigmann W. and Henry C.H. (1974) *Phys. Rev. Lett.* **33** 827

Dingle R., Gossard A.C. and Weigmann W. (1975) *Phys. Rev. Lett.* **34** 1327

Drummond T.J., Klem J., Arnold D., Fisher R., Thorne R.E., Lyons W.G. and Morkoc H. (1983) *Appl. Phys. Lett.* **42** 615

Duffield T., Bhat R., Koza M., DeRosa F., Hwang D.M., Grabbe P. and Allen S.J. (1986) *Phys. Rev. Lett.* **56** 2724

England P., Hayes J.R., Colas E. and Helm M. (1989) *Phys. Rev. Lett.* **63** 1708

Esaki L. and Chang L.L. (1974) *Phys. Rev. Lett.* **33** 495

Esaki L.and Tsu R. (1970) *IBM Jl. Res. Dev.* **14** 61

Esaki L. (1985) in *Proceedings of the 17th International Conference on the Physics of Semiconductors* (Eds. Chadi J.D. and Harrison W.A.) (Springer: New York)

Fasolino A., Molinari E. and Maan J.C. (1986) *Phys. Rev. B* **33** 8889

Fletcher K. and Butcher P.N. (1972) *J. Phys. C: Solid St. Phys.* **5** 212

Fuchs R. and Kliewer K. (1965) *Phys. Rev.* **104** A2076

Grondin R.O., Porod W., Ho J. and Ferry D.K. (1985) *Superlatt. Microstruct.* **1** 183

Harris J.J, Pals J.A. and Woltjier R. (1989) *Rep. Prog. Phys.* **52** 1217

Huang K. and Zhu B.F. (1988) *Phys. Rev. B* **38** 2183, 13377

Inkson J. (1984) *Many-Body Theory of Solids* (Plenum)

Inoue K., Sakaki H. and Yashino J. (1984) *Jpn. J. Appl. Phys.* **23** L767

Jain J.K. and Das Sarma S. (1989) *Phys. Rev. Lett.* **62** 2305

Joyce B.A, Dobson P.J., Neave J.H. and Zhang J. (1986) *Surf. Sci.* **174** 1; (1986) *surf. Sci.* **178** 110

Jusserand B. and Paquet D. (1985) *Superlatt. Microstruct.* **1** 61

Kim O.K. and Spitzer W.G. (1979) *J. Appl. Phys.* **50** 4362

Kittel C. (1953) *Introduction to Solid State Physics* (Wiley)

Klein M.V. (1986) *IEEE J. Quantum Electron.* **QE-22** 1760

Maraududin A.A., Montroll E.W., Weiss G.H. and Ipatova I.P. (1971) *Theory of Lattice Dynamics in the Harmonic Approximation* (Academic Press)

Marzin J. and Gerard J. (1989) *Phys. Rev. Lett.* **62** 2172

Munoz M.C., Velasco V.R. and Garcia-Moliner F. (1989) *Phys. Rev. B* **39** 1786

Nag B.R. (1980) *Electron Transport In Compound Semiconductors* (Berlin: Springer)

Nakayama M., Ishida M. and Sano N. (1988) *Phys. Rev. B* **38** 6348

Okumara H., Misawa S., Yoshida S. and Gonda S. (1985) *Appl. Phys. Lett.* **46** 4377

Osbourn G.C., Gourley P.L., Fritz I.J., Biefeld R.M., Dawson L.R. and Zipperian T.E. (1987) in *Multiquantum Wells, Selective Doping and Superlattices. Semiconductors and Semimetals* **24** (Ed. Dingle R.)

Palmier J.F. and Chomette A. (1982) *J. Physique* **43** 381

Ploog K. and Dohler G.H. (1983) *Advances in Phys.* **32** 285

Prange R. and Nee T. (1968) *Phys. Rev.* **168** 779

Prange R. and Girvin S. (1987) *The Quantum Hall Effect* (Berlin: Springer)

Ren S., Chu H. and Chang Y.C. (1988) *Phys. Rev. B* **37** 8899

Richter E. and Strauch D. (1987) *Solid State Commun.* **64** 867

Ridley B.K. (1989) *Phys. Rev. B* **39** 5282

Rode D.L. (1970) *Phys. Rev. B* **2** 1012

Ryan J.F., Taylor R.A., Turberfield A.J., Maciel A., Worlock J.M., Gossard A.C. and Weigmann W. (1984) *Phys. Rev. Lett.* **53** 1841

Ryan J.F. (1986) in *Two-Dimensional Systems: Physics and New Devices* (Eds. Bauer G., Kuchar F. and Heinrich H.) (Berlin:Springer)

Rytov S.M. (1956) *Soviet Physics -Acoustics* **2** 67

Sai-Halasz G.A., Esaki L. and Harrison W.A., (1978) *Phys. Rev. B* **18** 2812

Sakaki H., Noda T., Hirakawa K., Tanaka M. and Matsusue T. (1987) *Appl. Phys. Lett.* **51** 1934

Sawaki N. and Akasaki I. (1985) *Physica B* **134** 494

Seilmeier A., Hubner H.J., Abstreiter G., Weimann G. and Schlapp W. (1988) *Phys. Rev. Lett.* **59** 1345

Sibille A., Palmier J., Minot C., Harmand J. and Dubon-Chevallier C. (1987) *Superlatt. Microstruct.* **3** 553

Sibille A., Palmier J. and Minot C. (1989a) *Appl. Phys. Lett.* **54** 165

Sibille A., Palmier J.F., Mollot F., Wang H. and Esnault J.C. (1989b) *Phys. Rev. B* **39** 6272

Sibille A., Palmier J.F., Wang H. and Mollot F. (1990) *Phys. Rev. Lett.* **64** 52

Smith A.C, Janak J.F. and Adler R.B. (1967) *Electron Conduction in Solids* (McGraw-

Hill)

Smith and Mailhiot (1990) *Rev. Mod. Phys.* **62** 173

Sood A.K., Mendez J., Cardona M. and Ploog K. (1985a) *Phys. Rev. Lett.* **54** 2115

Sood A.K., Mendez J., Cardona M. and Ploog K. (1985b) *Phys. Rev. Lett.* **54** 2111

Tanaka M. and Sakaki H. (1987) *J. Crystal Growth* **81** 153

Tatham M.C., Ryan J.F., and Foxon C. (1989) *Phys. Rev. Lett.* **63** 1637

Tsu R. and Dohler G. (1975) *Phys. Rev. B* **12** 680

Tsuchiya T., Akera H. and Ando T. (1989) *Phys. Rev. B* **39** 6025

Vigneron J.P. (1988) in *Physics, Fabrication, and Application of Multilayered Structures* (Eds. Dhez P. and Weisbuch C.) (Plenum)

Warren G.J. (1988) *PhD Thesis*

Warren G.J. and Butcher P.N. (1986) *J. Semicond. Sci. Technol.* **1** 2133

Wataya M., Sawaki N., Goto H., Akasaki I., Kano H. and Hashimoto M. (1989) *Jap. J. Appl. Phys.* **28** 1934

von Klitzing K., Dorda G. and Pepper M. (1980) *Phys. Rev. Lett.* **45** 494